Development of a Versatile Raman Spectroscopy System

A thesis for the degree of

Master of Science

Submitted to

Dublin City University

By

Patrick Martin Byrne B.Sc.

Research Supervisor

Prof. Martin O. Henry

School of Physical Sciences

Dublin City University

February 1998

Declaration

I hereby certify that the material, which I now submit for assessment on the programme of study leading to the award of Master of Science is entirely my own work and has not been taken from the work of others save and to the extent that such work has been cited and acknowledged within the text of my own work

Signed Pat Byrne **ID Number** 95970606

Patrick Byrne

Date 5/2/1998

Table of Contents

Acknowledgements

I would like to thank my supervisor Prof Martin O Henry for the opportunity to pursue this interesting research and for his guidance and helpful suggestions during the course of this project I would like to thank Dr Enda McGlynn for his valuable help and support I would also like to thank Dr Conor McDonagh for many helpful discussions on different aspects of the research and Dr Ger O'Connor for allowing me the use of his laboratory and equipment at various stages during this project and his invaluable insights in the area of Raman spectroscopy

I am grateful to all my colleagues at DCU for their positive contribution to my time here, in particular Kate, Dirk, Shane, Will, Aidan, Mick, Ian and Mark A special thanks goes to the technical staff in particular Des and Alan for their expertise and patience

Thanks to all my friends outside DCU, including Donal, Tom, Fergal and Ann-Marie for their encouragement, humour and the distractions they provided

Finally I would like to thank my parents for their love, understanding and support which lifts my heart and lights my life, it is to them I dedicate this thesis

Abstract

This work describes the development of a facility for the analysis of materials, with particular interest in semiconductors, using Raman spectroscopy

In the apparatus described here a holographic notch filter was used to reject the Rayleigh scattered light, and two different spectrometers were evaluated for spectral analysis of the Raman signal The first spectrometer was a short focal length (0 1m) system and allowed a portable, compact device to be developed The second system used a 1m spectrometer for situations requiring high-resolution spectral analysis In both cases a Peltier cooled CCD detector was employed for signal collection The use of a fibre optic collection was investigated using the compact Raman system

The compact and high-resolution systems were both tested and characterised in terms of spectral resolution and response Different chemical and semiconductor samples were examined using both of these systems The particular materials were chosen to test the ability of these prototype Raman systems The results of the analyses performed are presented here

Chapter 1

Introduction

1 1 Introduction

Optical charcterisation of materials refers to the use of light to determine or examine the properties of a material The observation of how light interacts with a material through a number of different techniques can yield a great deal of information about the fundamental characteristics of the material The greatest advantages that optical methods have over other characterisation methods are that they allow non-contact, non-invasive and non-destructive testing of materials Optical methods also provide rapid feedback of analytical information, which allows essentially real-time analysis to be performed Taking semiconductors as a case in point, there are three main fields of characterisation electrical, physical/chemical and optical Electrical characterisation yields information about resistivity and carrier mobility and concentration but it requires the attachment of electrical contacts, which usually ends the further usefulness of the sample Physical characterisation such as scanning electron microscopy (SEM) and secondary ion mass spectroscopy (SIMS) can give information on structure, composition, defects and impurities The main drawbacks with these methods are the elaborate equipment and sample preparation required The specimen may also be altered during examination [1 1] Optical characterisation methods include

- Reflectivity and transmission, including ellipsometry, modulation spectroscopy and scatterometry
- Photoluminescence (PL) spectroscopy
- Infrared spectroscopy
- Raman scattering

The linear techniques mentioned in the first point allow the study of the electronic structure of solids via its influence on the optical constants The last three methods in particular can give information about such things as the lattice orientation, microstructure surface or interface, carriers, defects and impurities [1 2], [1 3]

The main advantages of optical techniques are

- Non-contact and non-destructive examination
- They do not require special environments, such as a vacuum
- Reduced sample preparation
- Allows spatial sampling of a specimen
- Provides real-time analysis

These extremely useful properties of optical characterisation methods make them particularly suited to on-line process monitoring and their use is becoming commonplace in a wide variety of industrial applications Developments in the area of lasers and detectors have made this possible

In particular recent advances in the area of Raman scattering [1 4] has allowed this optical technique to be applied to a diverse range of areas such as polymers, pharmaceuticals and semiconductors [1 5]

1.2 Light Scattering Spectroscopy

When light travels through a medium it obeys the law of conservation of momentum and is refracted or reflected However a tiny portion of the light is scattered in every direction by 'scattering centers' within the medium These points of scatter may be stationary or mobile depending on the nature of the inhomogeneity causing the scatter, examples of which include dislocations, density fluctuations and atomic vibrations Each of these sources of scatter has particular, identifiable types of scatter associated with them Of interest here is Raman scatter which is caused by a phonon-photon interaction, that is by vibrations interacting with light

1 2 1 Historical background

The first investigations of light scattering were carried out by Tyndall in the 1860's where he found that white light scattered at 90° by fine particles was partially polarized and slightly blue in colour Lord Rayleigh later derived an equation for the intensity of the scattered light The most important feature of this equation is the λ^4 dependence of the scattered intensity, this explains the blueness of the sky Rayleigh knew at this time that light is scattered by gas molecules and that dust particles were not necessary to give light from the sky its blueness and polarization

Three main components exist in light scattered by molecules or crystals Light that is scattered at the same frequency is said to be elastically scattered and is known as Rayleigh scatter, light scattered by density fluctuations associated with sound waves

(acoustic phonons) is known as Brillouin scattering, and light scattered by molecular vibrations within the medium (optical phonons) is known as Raman scattering Raman scattering and Brillouin scattering are both inelastic effects, that is, there is a change in frequency of the scattered light and they exhibit peaks of scattered light which are symmetrically placed on either side of the incident frequency A more detailed discussion of both effects may be found in [1 6]

The Raman components are typically shifted by between 100 and 4000cm^{1} from the exciting frequency, the scattered frequencies which are lower than the incident frequency are known as the Stokes components while the higher scattered frequencies are termed the anti-Stokes components Raman first observed these components in the 1928 [1 7] and was awarded the Nobel Prize for his pioneering work However, due to the weakness of the effect and the lack of suitable light sources not much work was carried out until the development of the laser in the 1960's

1.3 Developments in Raman Instrumentation

The measurement of a Raman spectrum requires a source of collimated and monochromatic light, ideally a highly parallel beam of one distinct wavelength such as that provided by a laser, a spectrometer to analyse the electromagnetic (EM) spectrum of the scattered radiation and a sensitive detector system An important consideration in the design of a Raman system is the difference in intensity between the Rayleigh scattered light and the Raman signal which is typically 8-10 orders of magnitude weaker Since the difference in frequency between these peaks in the spectrum may be only 1% of the excitation frequency, spectrometers for use in Raman spectroscopy must have two important properties, very good *spectral resolving power* and a very good *stray light rejection ratio*

Resolving power is given by $R=\lambda/\delta\lambda$ where $\delta\lambda$ is the wavelength difference between two spectral lines of equal intensity which are resolved Raman spectrometers typically have a resolving power of greater than 10^4 which can routinely be obtained using diffraction gratings

The stray light rejection ratio is defined as the ratio of the background stray light, that is light at all wavelengths other than the one of interest, to the signal Spectrometers typically have a stray light rejection ratio of between 10^4 to 10^6, which means that the intensity of this stray light can be orders of magnitude greater than the Raman signal Solutions to this problem involve the use of two or more spectrometers in series or the use of a "notch filter" to reject the laser light Double monochromators, which have

rejection ratios equivalent to the product of the ratios of the two monochromators, are widely used Triple spectrometers with multichannel detector systems are also common, in this case two monochromators are used in a "subtractive" arrangement as a notch filter with the third spectrometer providing the necessary dispersion to analyse the Raman spectrum

Recent technological developments in areas of each of the component parts necessary to the Raman system has allowed these systems to advance from large, stationary and delicate pieces of equipment, which were traditionally restricted to research laboratories, into compact, portable and rugged devices suitable for the industrial environment

When C V Raman carried out his investigations of vibrational scattering he recorded the spectra of liquids such as benzene and cabontetrachloride using a mercury arc lamp, a spectrometer and a photographic plate At that time a 24-hour exposure was required to obtain a measurable spectrum In the 1950's a new light source was developed called the "Toronto arc" which achieved up to 50 watts in the 435 8 nm emission line of mercury Even though only a small portion of this power could be applied to excite a sample it represented a major step forward However within a decade a true revolution occurred with the advent of laser sources that gave highly monochromatic light, which could be collimated, directed and focussed to give unprecedented power densities at the sample

The study of semiconductors using Raman scattering only became feasible when lasers became available, as most semiconductor materials are opaque at visible wavelengths Therefore it was necessary to either excite at a more suitable wavelength which would give a greater penetration depth and thereby a greater effective sample volume or increase the power density in the sample to yield measurable signals

Originally the He-Ne laser was used as a high power continuous wave laser for the generation of spontaneous Raman scatter This was replaced by Nd Yag, Ar^+ and Kr^+ lasers, which have a number of high power emission lines in the near infrared (NIR), and visible region of the spectrum There have been considerable advances in the production of lasers in recent years, most significantly the development of diode lasers operating at a variety of wavelengths from the visible to the NIR

The most important advances for Raman instrumentation have occurred in the areas of detector technology and holographic filter design

The photomultiplier tube (PMT) can be considered as a first generation detector, it is a single channel device with dark counts of $\approx 10\ s^{-1}$ The next generation systems were

optical multichannel analysers (OMA) which offer the advantage of *multichannel detection*, which can interrogate a number of different wavelengths simultaneously These devices enjoy improved sensitivity, greater dynamic range and real-time response A large number of different devices are catagorised as OMA's These include secondary electron conduction (SEC) cameras, silicon intensified target (SIT) detectors, photodiode array (PDA) or intensified photodiode array (IPDA) detectors and charge-coupled device (CCD) detectors A detailed discussion of these devices is given in [1 8]

The latter two devices have become most popular for spectroscopic applications, in particular the CCD due to it's high quantum efficiency (Q) and low dark rate In addition, the range of CCD's has been extended further into the blue by the use of scintillating coatings and "back-thinned" devices which also exhibit higher Q

Filter technology has also come a long way from the time of Raman's first experiments When mercury line sources were used to excite Raman scatter, mercury vapour cells could be placed between the sample and the spectrometer to absorb the unwanted Rayleigh scatter Similarly, iodine was used in conjunction with the 514 5 nm line of the argon-ion laser as it has a sharp absorption peak at that point in the spectrum Although these molecular gas absorption filters could achieve up to a 10^3 attenuation of the Rayleigh line, they had some unwelcome side effects such as secondary absorption peaks in the area of interest and fluorescence from the vapour cells themselves which could effect the Raman signature The use of a double monochromator with subtractive dispersion became the most popular method of filtering out the Rayleigh scatter, having the advantage of variability in wavelength and bandpass [1 9] however the throughput of these devices was at most 20% and their size and complexity made them suitable only for laboratory situations Other optical absorption filters include J-aggregate dye filters and ternary semi-conductor compounds such as $AgGaSe_2$ [1 10] Optical interference filters using multi-layer thin film dielectric materials are quite common, these band reject (BR) filters have an optical density (OD) of up to 4 at the laser line with transmission of over 60% outside the reject band but this may be modulated by up to 40% by interference effects which can be troublesome The latest development involves holographic filters [1 11] which show similar performance to interference filters but do not display modulation of their transmission outside the rejected band The latest generation of these holographic filters have an OD of greater than six within the reject band which is approximately 10 nm (<350 cm) wide and have a transmission of over 70% outside of this band [1 12]

Another area of development within the field of Raman Spectroscopy is Raman microscopy which was originally proposed in 1966 [1 13] and by 1974 the first instruments were developed One of these instruments was referred to as the MOLE (Molecular Optical Laser Examiner) [1 14] and was built around a conventional optical microscope coupled to a double spectrometer with mono or multi-channel detection This instrument provided both single point analysis and Raman imaging More recent developments in this area involve the use of line illumination and confocal optics

When taken together all of these advances have brought Raman instrumentation to a new plateau and the improvements in the latest generation of Raman systems have opened up new avenues of research and applications which previously could not have been considered

1.4 Concluding Remarks

This chapter gave a brief introduction to the origins of Raman spectroscopy and outlined the developments that have occurred in instrumentation for Raman spectroscopy up to the present day

Chapter 2 contains an introduction to the theory of Raman scattering and a discussion of a variety of application areas of Raman spectroscopy

Chapters 3 and 4 contain details of the development of two Raman systems and the results obtained with both systems

Chapter 5 contains conclusions drawn from the research and suggestions for further work that should be carried out

Chapter 2

Theory and Applications

2.1 Theory of Raman Scattering

A rigorous treatment of Raman theory is not presented here Rather an intuitive model is developed from the classical theory with the limitations of this theoretical model corrected for by the application of a basic quantum mechanical approach More rigorous and complete treatments may be found in [2 1], [2 2] and [2 3]

The Raman effect can be described as the inelastic scattering of light by matter When a visible photon interacts with a molecule it can be scattered in three ways It may be elastically scattered and retain the same energy it had before the interaction or it may be inelastically scattered by either gaining energy from, or losing energy to, the molecule during the interaction Photons that lose energy experience Stokes scattering, the energy being taken up by the molecule as vibrational energy Anti-stokes scattering is the term used to describe the situation where a molecule has excess vibrational energy which is imparted to the scattered photon

2 1.1 Classical Theory of Light Scattering

The classical description of the Raman effect regards the scattering molecule as a collection of atoms undergoing simple harmonic vibrations and does not take account of the quantisation of the vibrational energy When a molecule is placed in an electric field its electrons are displaced relative to its nuclei which develops a dipole moment If we assume the entire molecule is in a uniform incident electric field ε_{in} and that the incident light is monochromatic with frequency ν_{in}, the electric field may be expressed in the following form

$$\varepsilon_{in} = \varepsilon^{0}\mathrm{Cos}2\pi t\nu_{in} \qquad (1)$$

This incident light will induce an oscillating dipole μ which will re-emit (scatter) light at the dipole oscillation frequency For small fields this induced dipole is proportional to field strength ε_{in}

$$\mu(t) = \alpha\varepsilon_{in}(t) \qquad (2)$$

where α is the polarisability of the molecule (a measure of the ease with which the electron cloud may be distorted by the presence of an external electric field)

If the case of a diatomic molecule is considered, where the molecule vibrates with a frequency ν_v and if simple harmonic vibration is assumed, then the coordinate q_v along the axis of vibration can be described at a time t by the following equation

$$q_v = q_0 \text{Cos } 2\pi\nu_v t \tag{3}$$

The polarisability is a tensor quantity, which changes with time due to rotation in the case of *anisotropic* molecules, the tensor may also change when the molecule changes shape due to its vibrational motions If we consider the one dimensional case described above then the tensor form reduces to a scalar and for small vibrational amplitudes this change in polarisability will be given by

$$\alpha = \alpha^0 + \left(\frac{\delta\alpha}{\delta q_v}\right)_0 q_v \tag{4}$$

By substituting q_v from equation (3) into equation (4) the following expression for α is obtained

$$\alpha = \alpha^0 + \left(\frac{\delta\alpha}{\delta q_v}\right)_0 q_0 Cos 2\pi\nu_v t \tag{5}$$

By substitution of equation (1) into equation (2), the dipole induced by incident radiation of frequency ν_0 is

$$\mu = \alpha\varepsilon_{in} = \alpha\varepsilon^0 Cos 2\pi\nu_0 t \tag{6}$$

Finally if this molecule is vibrating with frequency ν_v, from equations (5) and (6) the dipole induced may be expressed as

$$\mu = \alpha\varepsilon^0 Cos 2\pi\nu_0 t + \left(\frac{\delta\alpha}{\delta q_v}\right)_0 \varepsilon^0 q_0 Cos 2\pi\nu_v t Cos 2\pi\nu_0 t \tag{7}$$

This can be rewritten as

$$\mu = \alpha\varepsilon^0 Cos 2\pi\nu_0 t + \left(\frac{\delta\alpha}{\delta q_v}\right)_0 \frac{\varepsilon^0 q_0}{2}\left(Cos 2\pi(\nu_0 + \nu_v)t + Cos 2\pi(\nu_0 - \nu_v)t\right) \tag{8}$$

The first term in equation (8) describes the Rayleigh scatter where the scatter frequency $\nu_{sc}=\nu_0$, the remaining terms describe the Raman scatter where $\nu_{sc}=\nu_0\pm\nu_v$ This equation shows that for Raman scattering to occur the polarisability must change during the vibration, that is

$$\left(\frac{\delta\alpha}{\delta q_v}\right)_0 \neq 0 \tag{9}$$

for the vibration to be *Raman active*

Equation (8) predicts the relative weakness of the Raman effect compared to Rayleigh scatter since the polarisability would be much larger than its derivative Since there is a λ^4 dependence involved in light scattering the difference classical theory predicts that the intensity of the anti-Stokes scatter should be greater than that of the Stokes scatter, however it is usually the Stokes scatter which is much stronger This is one of the discrepancies of classical theory which may be corrected for by the application of quantum mechanics

2 1 2 Quantum-Mechanical Theory of Light Scattering

Quantum theory recognises that the vibrational energy of a molecule is quantised The energy of each vibration for a harmonic oscillator will be quantised according to

$$E_v = h\nu(m+½) \qquad (10)$$

Where ν is the frequency of the vibration and m is the vibrational quantum number controlling a particular vibration Essentially the interaction between an EM wave and the molecule is treated as a perturbation of the molecule's ground state into a vibrational excited state with an energy gap corresponding to the perturbing wavefunction This is illustrated in the energy level diagram shown in Fig 2 1 with the vibrational transitions occurring through virtual energy levels

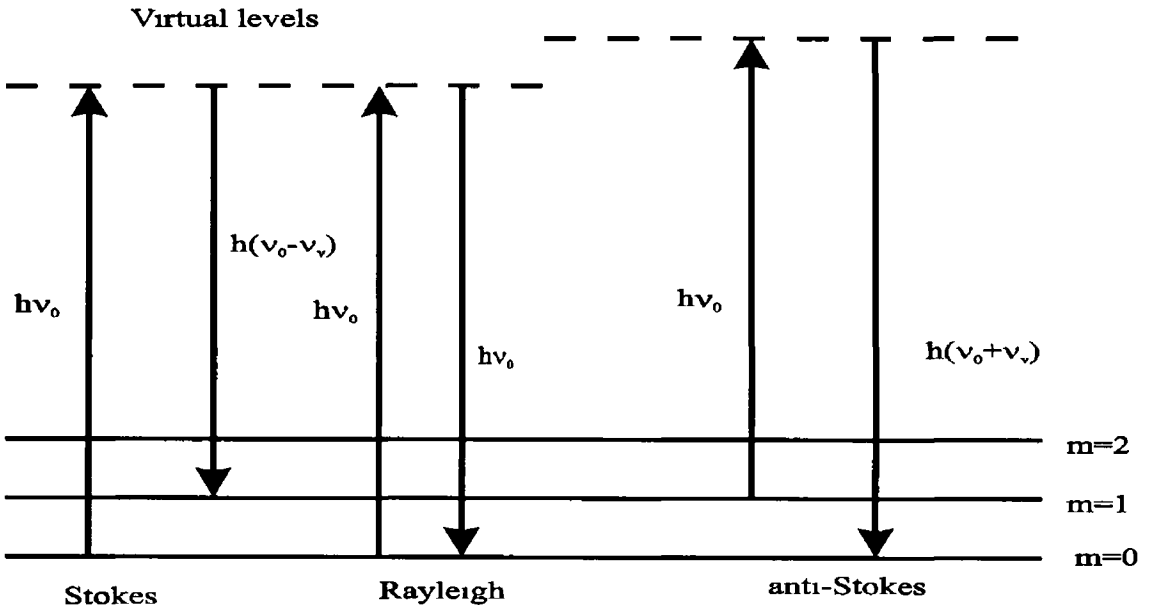

Fig 2 1 Energy level model for Raman scattering

The transitions that originate and terminate at the same vibrational energy level result in Rayleigh scatter Stokes Raman scatter arises from transitions originating at the ground

state and finishing at a higher level, whereas anti-Stokes involves a transition from higher to lower vibrational energy levels At room temperature most of the molecular vibrations are in the ground state, thus Stokes transitions are more likely than anti-Stokes This dependence upon the population of the vibrational energy level is seen experimentally in the relative intensities of the Stokes and anti-Stokes bands, as an example, the Raman spectrum of carbon tetrachloride shown in Fig 2 2

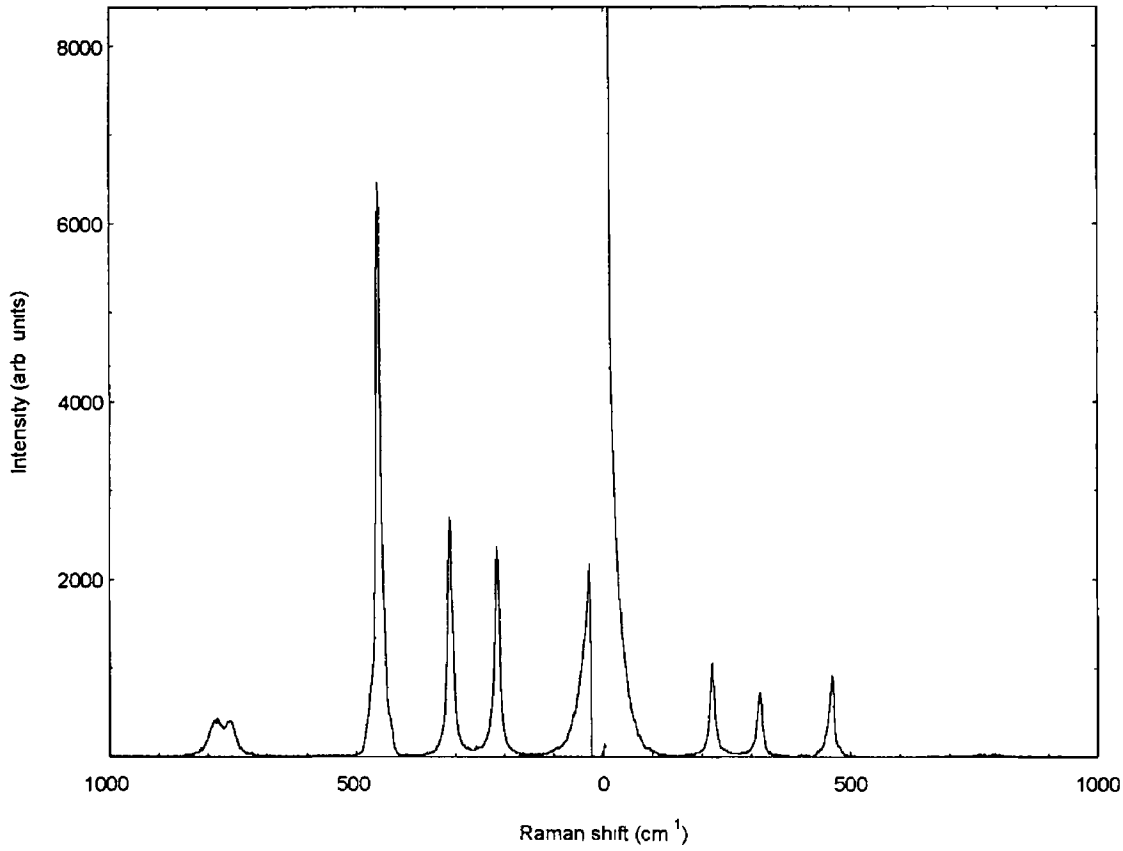

Fig 2 2 Stokes and anti-Stokes Raman spectrum of carbon tetrachloride showing the Stokes bands to be stronger than the anti-Stokes bands

2.1 3 Raman Intensities

Placzek's polarisability theory [2 4] leads to a semi-classical approach to the derivation of Raman intensities This theory applies to non-rotating molecules with a single ground state and with exciting light frequencies much less than electronic transitions of the molecule The intensity of the Stokes Raman band of shift frequency ν, scattered from an initial vibronic state m to a final state n is given by

$$I_{mn} = AI_0(\nu_0 - \nu)^4 \sum_{ij} \left|(\alpha_{ij})_{mn}\right|^2 \qquad (11)$$

where I_0 is the incident intensity, α_{ij} represents the components of the polarisability tensor associated with the transition from m to n, ν_0 is the frequency of the incident

excitation and A is a constant of proportionality Equation (11) shows both the wavelength dependence of scattered radiation intensity and the dependency of this intensity on the population of the vibronic states when multiplied by the number of molecules in state m

2 1 4 Selection Rules

The number of vibrational modes of a molecule may be calculated from the number of atoms in the molecule and whether it is linear or not However not every mode gives rise to a distinct band in the Raman spectrum, for the following two reasons

- For symmetry reasons, the incident light may not be able to induce transitions between levels of a given vibrational mode These modes are said to be *Raman inactive*
- Two or more Raman active modes may be *degenerate*, that is they have equal energy spacing and thus result in Raman scatter of the same frequency

The most useful method for predicting whether a mode is active or degenerate employs group theory, the details of which are beyond the scope of this document Measurement of the *depolarisation ratio* offers a useful method for determining the symmetry of a given vibration, only "totally symmetric" vibrations such as symmetric stretching modes give polarised Raman scatter from freely rotating molecules

2 1 5 Scattering Efficiency

For a comparison of the various optical processes such as absorbance, fluoresence and Rayleigh and Raman scatter a common measure of the efficiency of each process is necessary The measure used is the *cross section*, σ or the *differential cross section* $d\sigma/d\omega$ The scattering cross section may be defined using the equation

$$P_{sc}=\sigma_{sc}E_{in} \tag{12}$$

where P_{sc} is the rate of scatter in all directions from a molecule (in Watts) and E_{in} is the incident irradiance (Wm^{-2}) σ_{sc} may be thought of as the area presented by the molecule for scattering (m^2)

The rate of scatter can be calculated from the scatter intensity as

$$P_{sc} = 2\pi\int_0^{\pi} I_{sc}(\theta)\cos\theta d\theta \tag{13}$$

The differential scattering cross section $d\sigma/d\omega$ is the ratio of the light scattered at a certain angle θ to the incident light

$$d\sigma/d\omega = I_{sc}(\theta)/E_{in} \tag{14}$$

Process	σ (cm^2)
Absorption (UV)	10^{-18}
Absorption (IR)	10^{-20}
Fluoresence	10^{-19}
Rayleigh scatter	10^{-26}
Raman scatter	10^{-29}

Table 2 1 Typical values for cross sections, σ, for various interactions of incident EM radiation with molecules

It should be noted that the value of $d\sigma/d\omega$ (m^2sr^{-1}) varies with angle θ

Table 2 1 shows a comparison of typical values for cross section σ for different optical interactions, the relative weakness of the Raman process is obvious from this

2 1 6 Enhanced Scattering

This inherent weakness of the normal or *spontaneous* Raman effect is due to the inefficiency of promoting the molecule into a virtual state as shown in Fig 2 1 There are methods for improving the Raman scattering efficiency and these enhanced Raman methods can result in a significant increase in Raman scatter relative to the normal Raman effect

2 1 6 1 Resonance Raman Scattering

Resonance Raman scattering involves the use of excitation radiation of a frequency that coincides with an electronic transition of the scattering molecule, with the result that the excited electronic state contributes strongly to the scattering process Equation (11) indicates the relationship between the polarisability tensor and the Raman intensity When the electronic states of the molecule are considered the following expression for the change in polarisability α caused by the transition from m → e → n, where i and j are the polarisability tensor components, can be derived (adapted from [2 5])

$$(\alpha_{ij})_{mn} = \frac{1}{h}\sum_{e}\left(\frac{M_{me}M_{en}}{(\nu_{me}-\nu_0)+i\Gamma_e}+\frac{M_{me}M_{en}}{(\nu_{en}+\nu_0)+i\Gamma_e}\right) \qquad (15)$$

The summation here is taken over the excited state of the molecule e, while m and n denote the initial and final vibrational levels of the electronic ground state g M_{me} and

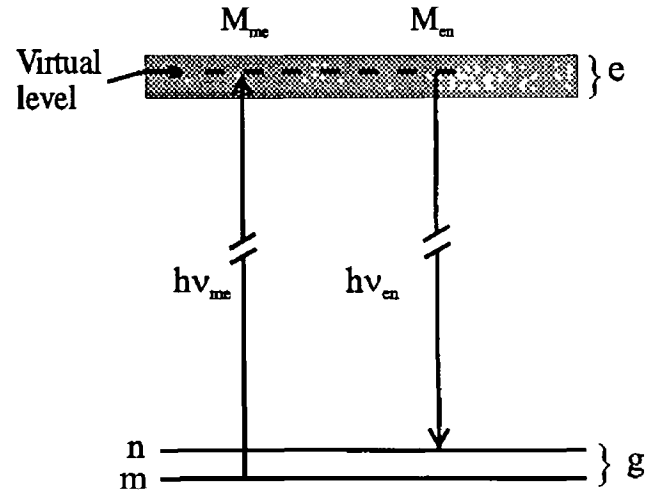

Fig 2 3 Energy level diagram for a resonance Raman transition

M_{en} are the electric dipole transition moments as indicated in Fig 2 3, for example

$$M_{me} = \int \Psi_m^* \mu_i \Psi_e d\tau \tag{16}$$

where μ_i is the i component of the electric dipole moment and Ψ is the wavefunction The excitation frequency is ν_0 and ν_{me} is the electronic transition frequency It can be seen that as ν_0 approaches ν_{me} the value of the first term of the polarisability tensor will increase rapidly Hence when this "resonance term" becomes large the intensity of the Raman band at ν_0-ν_{me} increases dramatically It should be noted that $i\Gamma_e$ is a damping term which prevents the denominator reaching zero

The Resonance Raman effect can cause an increase in scattering cross section of up to 10^6 for certain vibrational modes, only modes coupled to electronic transitions are enhanced Figure 2 4 shows a schematic comparison of the processes involved in normal Raman and resonance Raman scattering

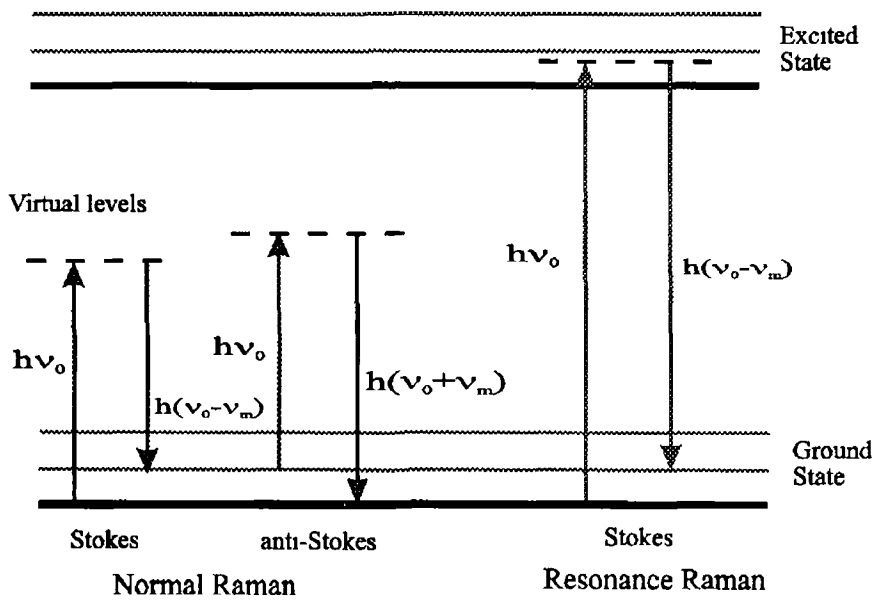

Fig 2 4 Comparison of the energy levels for normal Raman and resonance Raman

2 1 6 2 Surface-enhanced Raman Scattering

Surface enhanced Raman scattering (SERS) refers to a field of Raman spectroscopy concerned with molecules adsorbed onto metal surfaces The first report of this effect by Fleishmann *et al* [2 6] caused a great deal of interest due to the huge enhancement of Raman signal that they observed Enhancements of up to a million were observed for molecules adsorbed onto metal surfaces with submicron protrusions compared with nonadsorbed molecules The enhancement comes from a combination of electromagnetic and chemical interaction between the metal and adsorbed molecule

The electromagnetic effect is mainly due to surface plasmons in the metal being excited by the incident radiation, at the plasmon frequency large local fields occur on the surface which increase the Raman emission intensity The chemical effect is due to the overlap of metal and adsorbate wavefunctions, which causes charge transfer processes to occur In general the chemical effect is very short ranged (of the order of an Angstrom) and highly dependent on the energy levels of the adsorbate and so is material specific

2.2 Applications of Raman Spectroscopy

2 2.1 Materials Science

Raman spectroscopy is useful for the characterisation of materials and for the detection and identification of contamination and defects in materials In commercial production processes various contamination and defect formation problems are constantly encountered The identification of these contaminants or defects is critical to finding the source of the problem and hopefully solving it The fact that Raman spectroscopy can provide a molecular "fingerprint" of organic and inorganic materials makes it ideal for this type of detective work

2 2 1 1 Semiconductors

The non-destructive nature and high spatial resolution of Raman spectroscopy makes it ideal for characterising semiconductor materials and devices Raman spectroscopy is well suited as an *in situ* probe of semiconductor surfaces and interfaces [2 7] and has been used successfully to determine the molar composition of ternary semiconductor alloys [2 8] and to investigate the carrier concentration and space charge region in GaAs [2 9], [2 10]

Device structures fabricated by growing single crystal silicon on insulating substrates are of interest for very large scale integration (VLSI) due to an improvement

in the isolation between closely spaced devices when compared with bulk silicon material The quality of the crystal is paramount to the electrical properties of the devices so nondestructive examination of the processed material is necessary Raman scattering has been used to map the stress occurring in silicon-on-sapphire device structures [2 11] and to determine the crystal orientation in laser annealed silicon [2 12] Raman scattering is also useful for studying stress and crystal orientation in laser-crystallised silicon, which is of interest to the manufacture of silicon on insulator structures [2 13] Analysis of interdiffusion of atomic species at semiconductor interfaces has been presented [2 14], this analysis requires the ability to monitor the heterostructure down to a single atomic monolayer

As semiconductor devices and components become smaller and more complex, material contamination and processing flaws become more significant Raman microprobe analysis can provide information about the molecular structure of particles to sub-micron dimensions This makes it perhaps the only suitable non-contact method for identification of contamination of this nature [2 15]

Yet another application related to the semiconductor industry is the monitoring of processing baths The RCA cleaning process is widely used to remove contaminants from the Si wafer surface The Standard Cleaning 1 (SC1) solution, one of the most common RCA cleaning solutions, is comprised of an $NH_4OH/H_2O_2/H_2O$ mixture This is an extremely corrosive and unstable solution, which can damage the Si surface and thus reduce product yield This damage to the surface occurs due to the instability of the SC1 solution as the etch rate of the silicon varies with the composition of the solution [2 16] This situation necessitates the real-time monitoring and control of the solution composition which can be achieved using Raman spectroscopy as the SC1 components are good Raman scatterers and can be simultaneously monitored with this technique, see Fig 2 5

2 2 1 2 Polymers and Glasses

Raman spectroscopy can be applied to the examination of industrial polymers, to identify defects and characterise molecular orientation and crystallinity Defects in polymer fibers or film are often caused by non-uniform distribution of copolymers or by inclusions These defects can impair the clarity of the material or cause mechanical instability Substances causing these defects can be identified and the source of contamination deduced, whether it is part of the production process or due to material handling Raman spectroscopy has also been applied to the study of polymer laminate

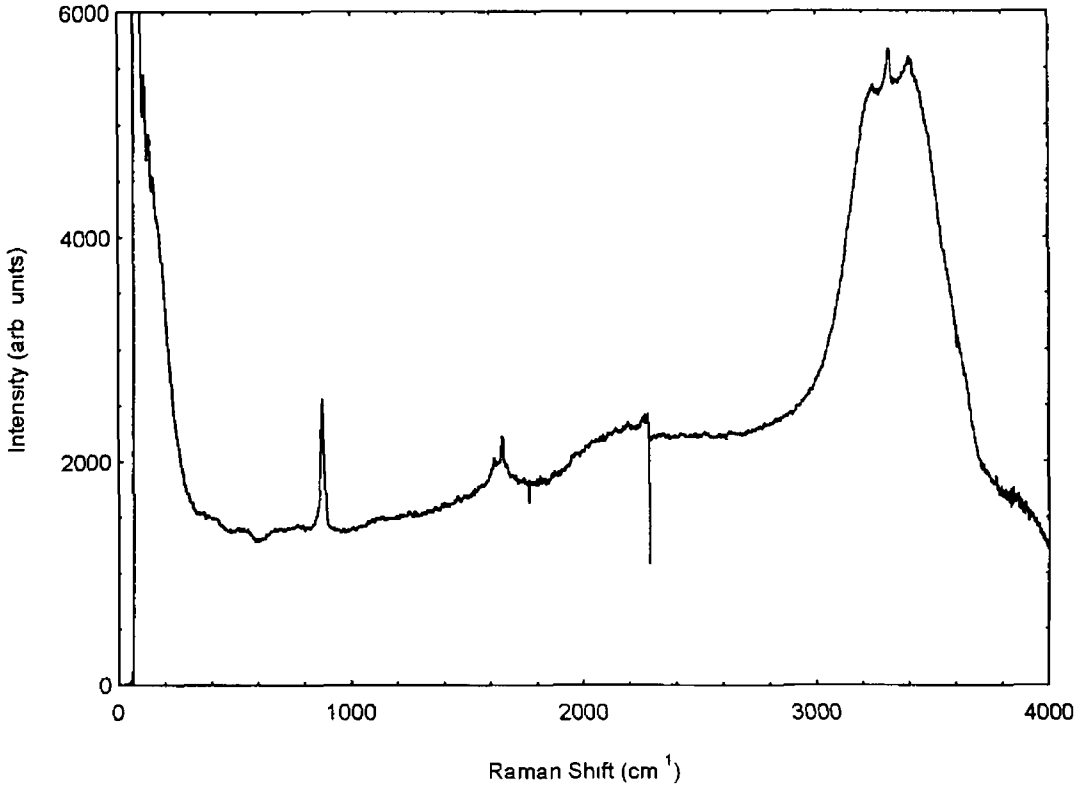

Fig 2 5 Raman spectrum of SC1 solution The Raman band of H_2O_2 can be seen near 880cm ^{1} and the sharp band from NH_4OH can be seen near 3315cm ^{1}

interfaces, the distribution of additives within a polymer and the degree of solubility of these additives [2 17] This technique can also be used to monitor chemical polymerisation processes and determine the degree of bulk polymerisation [2 18]

Commercial glass production can suffer from the formation of bubbles within the glass, these inclusions can be analysed to identify the material deposits present in the bubble [2 19] This information can then be used to select materials and processes that will inhibit the formation of such inclusions

2 2 2 Thin films and Adsorbed Species

Since the advent of the laser for use in Raman spectroscopy it was shown that spectra of molecules adsorbed on surfaces could be obtained and with the development of more sophisticated instrumentation even films of monomolecular thickness could be observed The many different sampling arrangements which have been used in the study of thin films fall into two basic configurations backscattering geometry or a grazing-incidence arrangement The backscattering geometry is more useful when dealing with film thickness in excess of 10 μm For thinner films, the first method proposed involved an incident angle of 70° to the surface normal for the laser excitation [2 20] This glancing incidence approach was shown to give useful spectra of benzoic acid depositions on silver down to 50Å thickness A more sophisticated approach [2 21] used

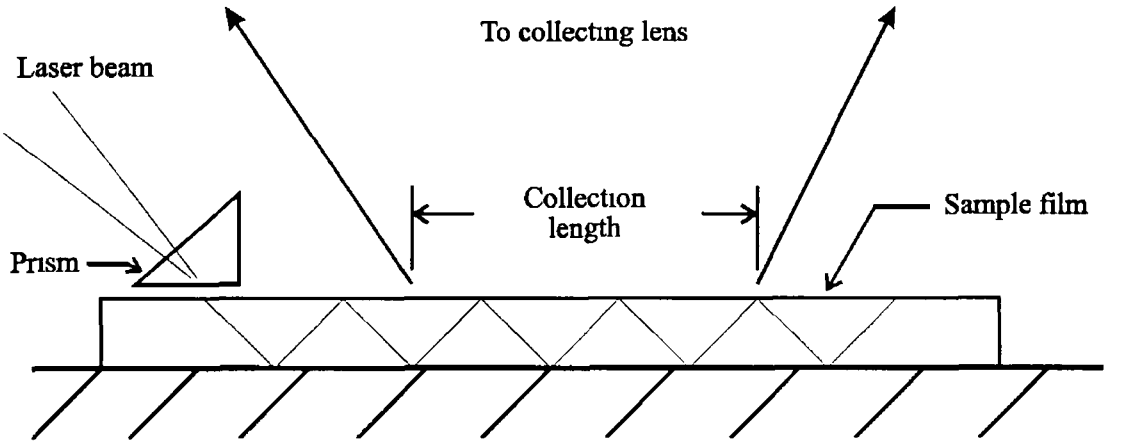

Fig 2 6 Application of the waveguide technique to Raman analysis of thin films (Reproduced from Fig 2 24 of Ref [2 22])

the film as a waveguide and coupled the laser into the film using a prism as shown in Fig 2 6 A more detailed discussion of this method and the conditions that apply to its operation can be found in [2 22]

The formation of titanium films on silicon has been characterised using off-axis illumination [2 23], which provided *in situ* monitoring during film deposition Subnanometer buried layers of germanium in silicon have also been characterised with Raman spectroscopy [2 24] Figure 2 7 shows the Raman spectrum of carbon nitride films obtained using a commercial Raman microprobe [2 25]

A particularly useful attribute of Raman analysis in the investigation of carbon films is its ability to easily distinguish between carbon with sp^3-type bonding (diamond) and sp^2-type bonding (graphite and carbonaceous materials) The method and conditions of deposition will determine whether a thin film becomes crystalline diamond which has a characteristic Raman peak at 1332cm^{-1} or amorphous diamond-like carbon (DLC) which typically has a broad band at 1530cm^{-1} with a shoulder at about 1400cm^{-1} in its Raman spectrum [2 26] This ability to distinguish between these two types of carbon film is shown in Fig 2 8

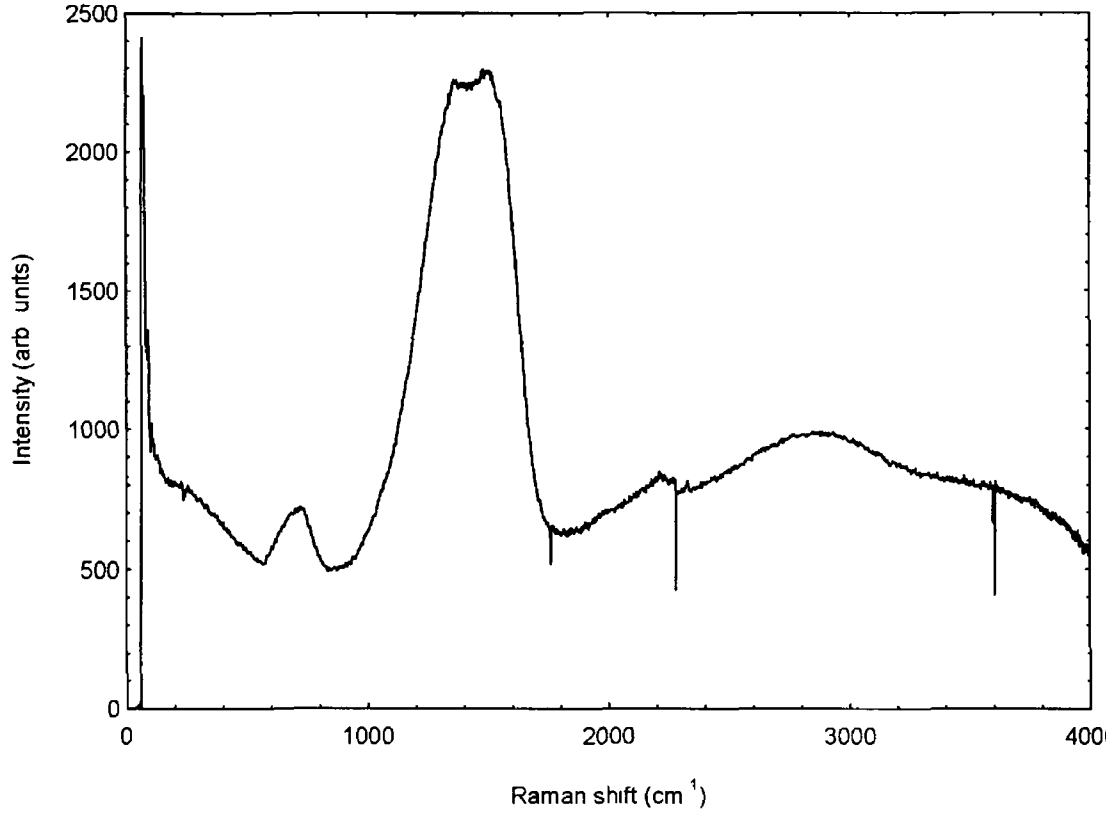

Fig 2 7 Raman spectrum of a carbon nitride thin film on a silicon substrate

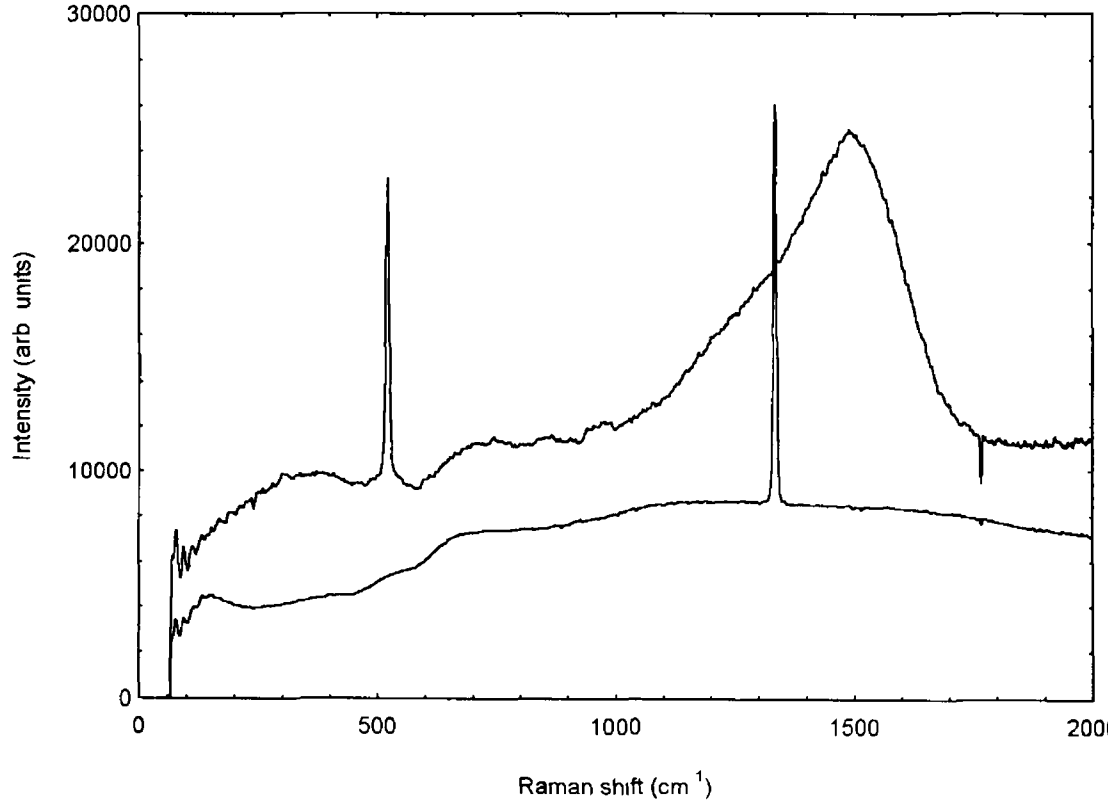

Fig 2 8 Comparative spectra of crystalline diamond with a sharp peak at 1332 cm ^{1} and amorphous DLC grown on a silicon substrate showing a broad peak as described in the text The sharp peak of the silicon substrate at 520cm ^{1} is also observed

2 2 3 Geology and Mineralogy

The *in situ* Raman analysis of fluid inclusions in minerals can yield information related to the geological processed involved in the formation of the host mineral This technique has also been applied to the examination of gems, particularly transparent gems which may be examined in setting, which can reveal details about the identity and origin of the gem Natural and synthetic gems may be distinguished in this manner [2 27]

2 2 4 Environmental Detection

The micro-Raman technique has been used for the identification of airborne particles of 1-10μm in size, which is of particular interest to the area of pollution monitoring Results of the characterisation of airborne dust in an urban environment have been presented [2 19] Raman spectroscopy is especially suited to the identification of organic compounds such as pesticides, insecticides, hydrocarbons and common inorganic minerals like silicates, carbonates, sulfates and oxides Power plant emissions and stratospheric aerosols have also been characterised in this way

2 2 5 Biology and Pathology

The Raman microprobe has facilitated the molecular investigation of biological samples at the cellular level, although traditionally biological specimens could only be examined in regions of high sample concentration due to the low power densities required to avoid damaging the sample Raman spectroscopy has been used to examine liver cells infected with hepatitis and to show accumulation of a drug in the liver The technique has also been applied to the examination of "blue particles" found in cancerous cells which have proved identical and independent of the origin of the cancer [2 28] The resonance Raman effect has been employed to examine structures in plant and animal cells Since the scattering cross-section is low for normal Raman scattering in these samples and strong fluorescence is observed, excitation with near-infrared radiation (NIR) has been utilized to avoid the fluorescence problem The most promising advance for biological samples is the use of SERS-active substrates which increases the sensitivity and simultaneously reduces the fluorescence

2 2.6 Food and Pharmaceutical Industries

Drugs are mixtures of many different particles, which may not be easily distinguished from one another by visual microscopy However, Raman micro-spectroscopy can record the spectra of each particle and thus identify it [2 28] This can

be put to good effect either to monitor composition or for product identification [2 29] which may even be accomplished through packaging material

Raman spectroscopy has also proven useful for monitoring of the degree of unsaturation of edible fats and oils [2 29], which is of interest to the food industry for process quality control and nutritional labeling The spectra shown in Fig 2 9 illustrate the ability to measure the unsaturation which is proportional to the intensity of the C=C stretching vibration at about 1660cm ^{1}, the saturation is greater for butter than margarine as can be seen here

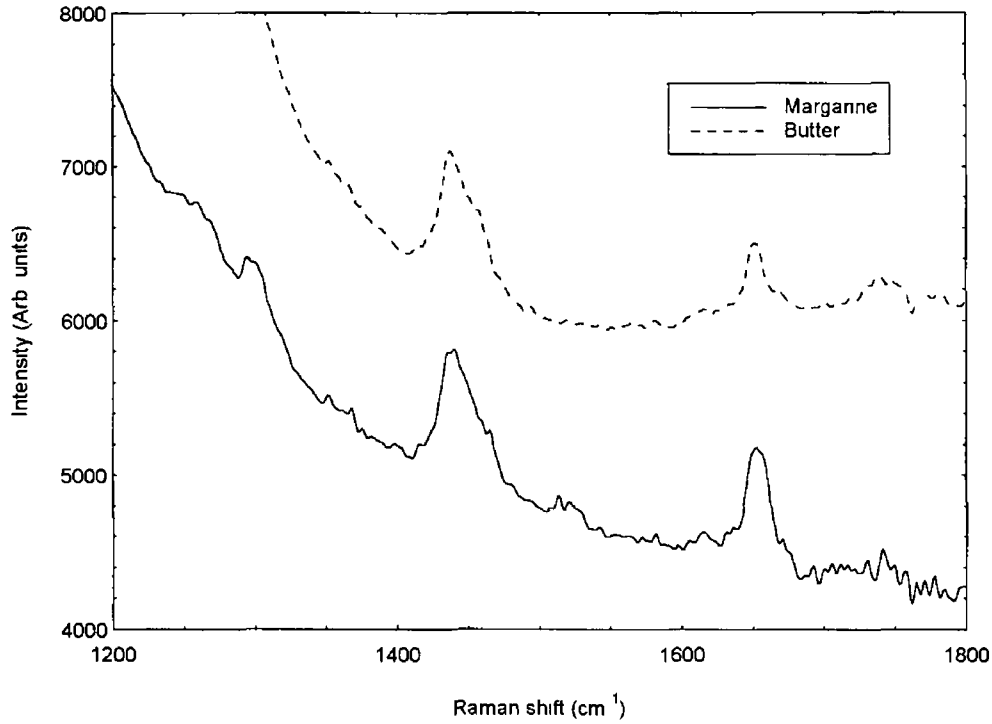

Fig 2 9 Comparative spectra of butter and margarine showing relative intensities of C=C stretching peak at 1660cm ^{1}

2.3 Conclusion

This chapter contains an introduction to the theory of Raman scattering through a classical and very basic quantum mechanical approach There is also an introduction to the concepts of Raman intensity, selection rules and scattering efficiency, which are of importance to the collection and analysis of Raman signals The wide range of research and industrial applications of Raman spectroscopy are presented

The next chapter describes the development of a Raman spectroscopy facility using cutting edge technologies to provide a compact and cost effective system

Chapter 3

Compact Raman system.

3 1 Introduction

This chapter describes the development of a compact Raman spectroscopy system Each component of the system is described, the pertinent design considerations are outlined and the configuration of the system is specified

The system was characterised and the results of these tests on the system, along with test spectra obtained are presented here

3.2 System components

3 2 1 Excitation source

As mentioned previously the most suitable light source for Raman spectroscopy is a laser There are certain considerations and constraints that must be taken into account when choosing a particular laser source Firstly one must consider the power requirements, as the Raman effect is so weak it is beneficial to have high powers available at the sample Secondly one must consider the wavelength of excitation that is most desirable, there are a few factors that influence this decision

- The wavelength of the source must be a reasonable match to the useful wavelength range of the detection system
- The wavelength dependence of the scatter intensity ($I \propto \lambda^{4}$) is important as it mitigates against the use of longer wavelength excitation
- Sample considerations, particularly if the sample exhibits fluoresence, which may be reduced by the use of near-infrared excitation or if the sample can be damaged by light or high temperatures caused by absorption at particular wavelengths

The laser source chosen for use in this Raman system was a continuous wave (CW) argon ion laser operating at 514 5 nm (Coherent Innova 70) This laser offers high power output at a wavelength which gives good Raman efficiency and falls within the gain curve of a silicon CCD detector This laser was water cooled and thus suitable for laboratory-based use There was also an air-cooled Ar^{+} laser available with sufficient power (up to 100 mW) in the 514 5 nm line, which would allow for system portability

3.2 2 Spectrometer

The spectrometer used for this compact system was an American Holographic model 100S spectrograph, illustrated schematically in figure 3 1 This small, lightweight spectrograph has a focal length of 100mm and an f/# of 2 5 It employs a concave, aberration corrected holographic diffraction grating, which is particularly suited for use with diode array or CCD detectors due to its flat focal field This spectrometer has interchangeable entrance slits and gratings, the grating used for this work was model 446 05/L, which has a central wavelength of 700nm and an average dispersion of 8nm/mm Two different slit widths were available, 100μm and 50μm, model numbers SL-0100 and SL-0050 respectively

The wavelength is selected by means of a locking micrometer, this micrometer is not wavelength calibrated so the system must be calibrated for each new wavelength range However the micrometer allows repeatable positioning of the grating, so a previously calibrated range may be returned to by adjustment to the recorded micrometer reading The procedure for calibrating the spectrometer/detector system is outlined in section 3 5 2

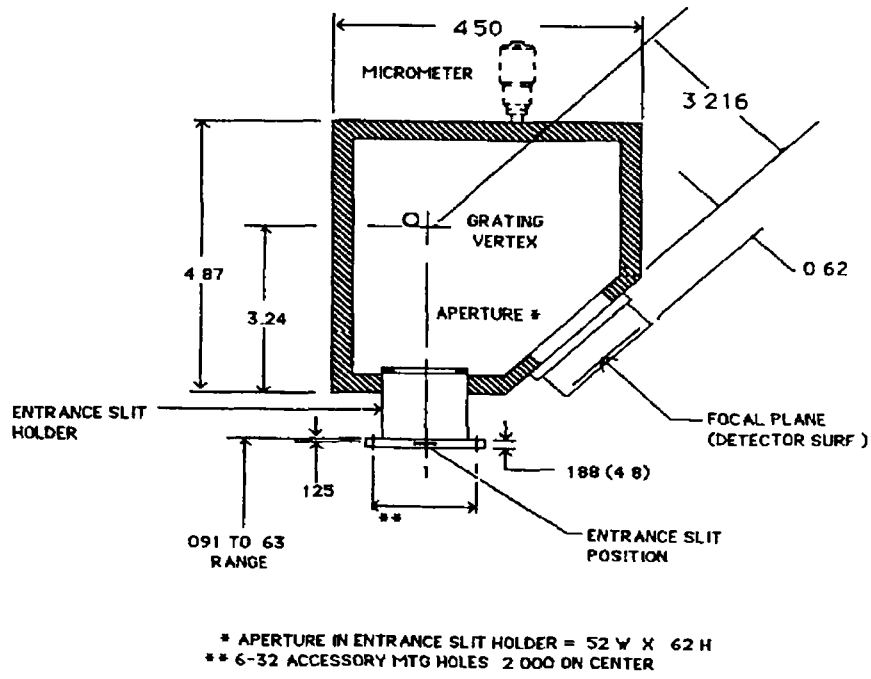

Fig 3 1 A diagram of the American Holographic model 100S spectrograph

3 2.3 Detector

The CCD detector offers many advantages as a detector system for use in Raman spectroscopy As outlined in section 1 3, these devices have low dark current, high signal/noise ratio, high efficiency and allow for the simultaneous observation of a range

of spectral wavelengths For these reasons the detector of choice was a CCD and the model used was an E G&G PARC OMA-Vision system with a Thomson CSF THX-31159A, front illuminated, four phase silicon CCD The wavelength range of this detector is 400nm-1000nm, with a quantum efficiency of approximately 35% in the area of interest (500-600nm) The sensor is comprised of an array of 1024×256 photo-elements of dimension 19μm×19μm This rectangular shape is particularly suited to spectroscopic applications The parameters of a CCD and its operation are described in section 3 2 3 1

3 2 3 1 Principles of CCD operation

A CCD is a two dimensional array of photo-sensors or photo-sites When the CCD is exposed to a spectral source, photons striking the image face generate charge in these photo-sites This charge accumulates while the CCD is exposed to the light This period of time is termed the exposure time When the light is blocked from the CCD, usually by means of an electronically controlled shutter, the charge that has built up in the photo-sites may be transferred from the device The technique used to transfer the charge in the CCD used here is known as *four phase shifting* and refers to the four buried electrodes under each photo-site These electrodes address each individual pixel and maintain the charge collected in each photo-site in independent potential wells When CCD's are used in dispersive spectroscopic applications, as opposed to imaging applications, it is usual that the pixels running in the direction of the spectral lines are grouped or *binned* to form a *superpixel* while maintaining maximum resolution across the spectrum Binning in this way forms a pseudo-PDA of 1024 superpixels each of 19μm × 4 86mm in dimension Binning may be carried out in a more precise manner by just using the rows of the CCD which are collecting a useful signal if the height of the spectral lines are not filling the detector area This avoids adding unwanted noise to the signal The technique of binning offers the benefit of increasing the signal to noise ratio (S/N) and reducing the readout time as it reduces the number of readouts to one for each binned column As readout noise is a significant source of noise in CCD operation, this technique is extremely useful for low signal applications Readout involves transferring the charge row by row into the *serial transfer register* or *shift register* Obviously when a column of pixels are binned together this essentially forms a single row for readout The charge packets are then shifted one by one along the shift register to the video output of the CCD chip This analogue signal is amplified and sent to the analogue to digital converter (ADC) where it is converted to an 18-bit digital format in the case of

the CCD operated here The ADC determines the dynamic range of the detector, in this case 2^{18} or 262,144 levels, that is, the signal may be specified by a discreet level from zero up to saturation, which corresponds to the highest level This digital information can then be displayed or manipulated as required

3 2 4 Holographic filter

The pivotal component of the Raman system is the filter that is used to block the Rayleigh scatter before the spectrometer The filter employed here is a Kaiser Optical holographic SuperNotch-Plus™ filter designed for operation at 514 5nm

This filter has a spectral bandwidth of 244cm ^{1}, an optical density of greater than 6 within the band stop of the filter and transmission of 75% on the Stokes side These attributes make it ideal for Raman spectroscopy and can allow useful spectra to be obtained to within approximately 100cm ^{1} of the exciting laser line [3 1]

A discussion of the fabrication process of this type of filter and its characteristics can be found in [3 2]

3.3 Design Considerations

3 3 1 Excitation focusing

Since the intensity of the Raman scatter is proportional to the irradiance (power/cross-sectional area) of the exciting beam it is extremely beneficial to focus the beam onto the sample The damage threshold of the sample of course limits the irradiance At the point of focus of the beam its diameter is limited fundamentally by the diffraction limit and by aberration effects as illustrated in fig 3 2 Thus the "beam waist", d, is given by

$$d = 4\lambda f/\pi D \qquad (3\ 1)$$

where λ is the wavelength of the excitation light, f is the focal length of the lens and D is the laser beam diameter The length of this focal cylinder is given by

$$L = 16\lambda f^2/\pi D^2 \qquad (3\ 2)$$

For a laser wavelength of 514nm and a typical beam diameter of 3mm, using a focusing lens of 60mm focal length, equation (3 1) gives the beam waist to be approximately 15μm This gives an increase in irradiance of over 10^4 compared to the unfocussed beam with a corresponding increase in Raman intensity The length of the focal cylinder in this case is of the order of 1mm from equation (3 2), which gives an

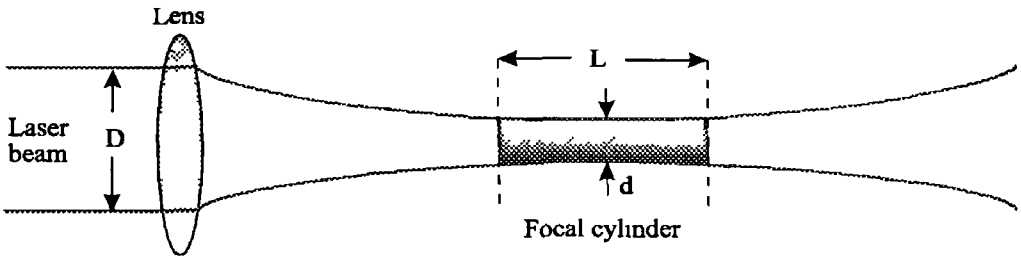

Fig 3 2 Diagram showing laser focusing, indicating the beam waist and the length of the focal cylinder

irradiated volume of about $10^{-7}cm^3$ The absorption length in the sample determines the irradiated volume

3 3 2 Collection geometry

There is as yet no definitive or standard collection geometry for Raman spectroscopy, the 90^0 and 180^0 (back-scattered) arrangements are preferred Traditionally the 90^0 geometry is preferred since it allows alignment of the focal cylinder of the laser with the long axis of the spectrometer slit This method is quite useful for transparent samples, however for samples with a small penetration depth the back-scattered geometry offers the best solution Both of these collection geometries were employed here depending on the nature of the sample Liquid samples were held in a quartz cuvette and the 90^0 geometry was used whereas for semiconductor samples the 180^0 method was employed The 90^0 geometry applied here involved *f/#* matching to the spectrometer and magnification to increase the collection angle ω at the sample as illustrated in fig 3 3a The back-scattered geometry as shown in fig 3 3b was used for solid samples, the deviation from true 180^0 illumination has little effect and in the case

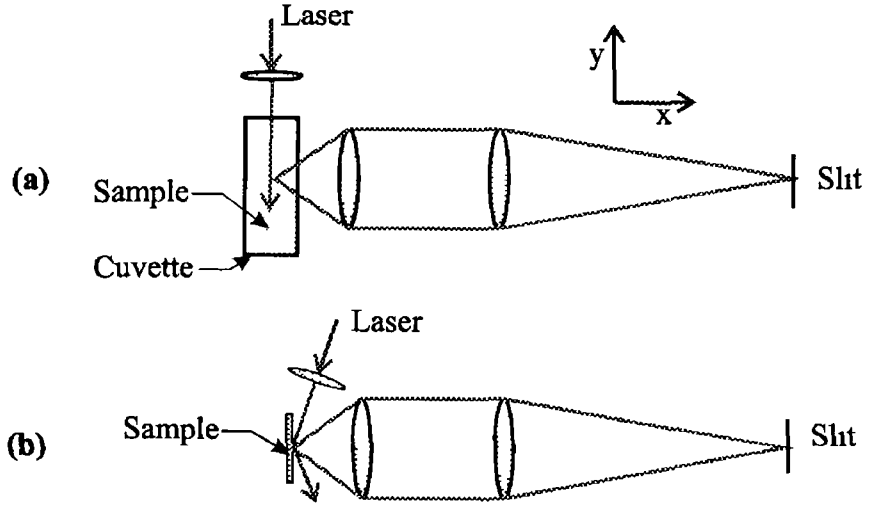

Fig 3 3 Schematic drawing showing collection geometries, (a) 90^0 geometry and (b backscattering or 180^0 geometry

of high refractive index materials it is effectively negated as the beam is refracted into the material Polarisation information was obtained by having the excitation beam polarised in the z direction An analyser was placed in the collection path This was set in the z or y direction to observe the scattered intensities corresponding to the polarisations parallel or perpendicular to the excitation respectively

3 3 3 Signal maximisation

The Raman signal is made up of a number of variables that may be divided into those determining the scattering intensity and those determined by the collection and detection of the scattered light The *specific intensity* of the scatter, also known as the *radiance*, is determined by the laser power density P_D, the scattering cross section β_a ($\beta=d\sigma/d\omega$) and the number density of molecules of the specimen under analysis D_a The collection and detection variables include the *entendue* of the system $A\omega$, which may be thought of as the maximum beam volume the instrument can accept, the transmission of the system T, the quantum efficiency of the detector Q and the exposure time t These variables may be brought together to give an equation for the signal as follows

$$\text{Signal} = (P_D\beta D_a)\,(A\omega TQt) \qquad (3\ 3)$$

From this equation it can be seen that the only factor of the specific intensity of the scattered photons which may be controlled is the laser power since the other factors are dependent on the sample The factors, which determine how many of these photons are detected, allow more scope for optimisation The transmission of the spectrometer and the quantum efficiency of the detector are inherent to the instruments, so careful choice of instrument is required to maximise these The exposure time may be varied as required up to the saturation level of the detector in order to obtain a measurable signal during the course of experimentation Ultimately the system *entendue* is the factor that must be maximised by careful design since it is determined by the least optimised segment of the entire optical system The $A\omega$ product is usually determined by the spectrometer *f/#* and the entrance slit area or the area of the detector, thus the collection optics should completely fill the spectrometer to make maximum use of the available $A\omega$ product However, overfilling the spectrograph may result in increased stray light and since this is a particular problem with a single monochromator it must be prevented

As mentioned previously the collection optics employed in this design matched to the *f/#* of the spectrograph (*f/#* = 2 5) and magnified the image of the sampling area onto the slit thus allowing an increased collection angle (*f/#* = 1) to maximise the solid angle of scattered light collected A trade off occurs here as the entrance slit apertures the

image of the sampled area, thus to optimise the flux entering the spectrometer the magnified image of the sampled area must match the entrance slit dimensions With a 50 μm slit in operation this necessitates a sample area of less than 20 μm wide, which obviously requires tight focusing of the laser beam In turn this makes alignment of the excitation beam and the slit image difficult

3.4 System configuration

This system was designed to allow a number of different configurations to be employed The system could be used with open optic or fibre optic signal collection as described below The Raman system was also made compatible with an existing system that allowed for whole wafer maps to be obtained This wafer mapping system used photoluminescence for uniformity mapping of wafers and was adapted to allow Raman scattering to be applied as well

3 4 1 Open optics

In the arrangement using open optics, the collection optic, holographic filter and delivery optic were positioned along the optical axis (z-axis) of the spectrometer such that the collected scatter from the sample was imaged onto the spectrometer slit after passing through the notch filter The collection lens used was an *f/1* plano-convex lens and the delivery lens was an *f/2 5, which* gave a magnification of 2 5 and matched effectively to the spectrometer's numerical aperture The holographic notch filter was 25 mm in diameter and this dimension essentially dictated the size of the other optical components, that is, all lenses used were 25 mm in diameter All optical components employed in the systems described here made use of broad band visible anti-reflection

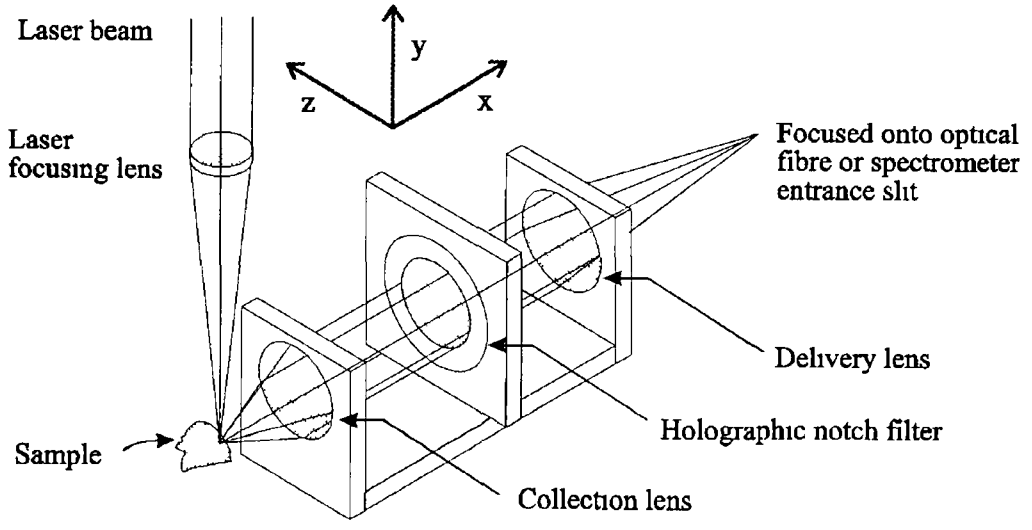

Fig 3 4 Diagram indicating optical arrangement, showing excitation and collection optics.

coatings to minimise reflection losses through the system

As mentioned in section 3 3 2 the sample illumination was along the y-axis to match to the long dimension of the spectrometer entrance slit as illustrated in fig 3 4

3 4.2 Fibre optic collection

In this configuration the spectrometer entrance slit was directly replaced with an optical fibre bundle This was a circular to rectangular fibre bundle of 1 m in length encased in stainless steel sheathing A special adapter was designed and fabricated which allowed the rectangular end of the fibre bundle to be mounted to the spectrometer and essentially become the spectrometer entrance slit The effective slit dimensions with the fibre bundle in place was 100 μm wide × 2 5 mm high The fibre bundle was made from high-grade fused silica, which has high transmission efficiency (60%) in the visible region, and had an *f/#* of 2 3 which allowed efficient *f/#* matching to the spectrometer The circular end of the bundle was terminated with an SMA connector and had an input aperture of 1 63mm in diameter The entire aperture area does not collect light due to the packing together of the cylindrical fibres, the efficiency of which is defined by the *packing factor* With this fibre in place the collection optics effectively became a filtered probe head with the delivery optic focussing the collected scatter onto the end of the fibre bundle The use of fibre optics in this way greatly simplifies the collection of light by the spectrometer The fibre bundle removes the necessity of aligning the collection optics with the spectrometer and all difficulties associated with this The fibre optic arrangement also provides a very efficient method of collecting the light into the spectrometer The fibre bundle allows the collection optics to move about independently of the spectrometer which is particularly useful in regard to the wafer mapping configuration described in the next section, 3 4 3

It was found that when the optical fibre was employed, readjustment of the entrance slit position was required to maintain optimum focus in the detector plane Details of this focussing procedure are given in section 3 5 1

3 4 3 Wafer mapping facility

The wafer mapping facility developed in this laboratory originally used photoluminescence for homogeneity mapping of semiconductor wafers The facility consisted of a cryostat, a computer controlled x-y translation stage, a spectrometer and CCD detector The illumination/collection optics consisted of a 90^0 off-axis parabolic mirror mounted on the x-y table and in the original configuration used an elliptical plane

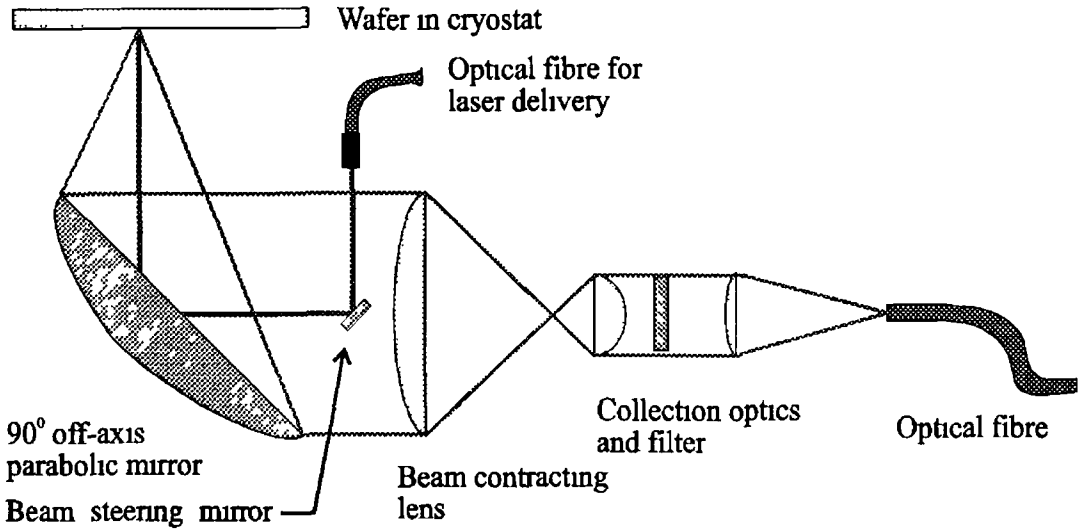

Fig 3 5 Schematic drawing of wafer mapping optical arrangement

mirror to maintain optical alignment as the parabolic mirror was scanned in the x and y directions [3 3]

The objective of this project in relation to the wafer mapping system was to extend its capabilities by carrying out the necessary modifications to allow this system to use Raman scattering analysis as a complementary technique to the existing photoluminescence analysis This was achieved by replacing the existing beam steering optics by the filtered probe head and fibre optic collection as described in the previous section This was designed to be used in conjunction with the parabolic mirror which was 75mm in diameter, thus it was necessary to employ a beam contractor to match the beam diameter from the parabolic mirror to that suitable to pass through the holographic filter The optical arrangement for this configuration is indicated schematically in fig 3 5

Other improvements to the system included the writing of a new control program to allow both the CCD and x-y stage to be controlled from a single computer and to properly synchronize the mapper translation with the collection of spectral data This is described in appendix A Also an excitation source compensation system was designed and built for use with the system, this is described in appendix B

3.5 Experimental Procedures

This section outlines certain procedures, which are vital to the setup of the system components before use or are relevant during operation of the system

3.5 1 Detector/Spectrograph Alignment

The use of the OMA4 CCD and 100S spectrograph combination in this system required that the detector and spectrograph be aligned before use as this was not a ready built or factory assembled system

There are two separate issues involved in the correct alignment of the system

- Focus adjustment
- Rotational adjustment

Focus adjustment or *in-out* alignment involves positioning the focal plane of the spectrograph so that it coincides with the detector surface With this spectrograph and detector combination this is achieved by adjusting the position of the entrance slit relative to the grating as the grating to detector distance is fixed The accurate positioning of the focal plane is critically important with this short focal length spectrograph, as the loss of resolution on the detector is dramatic for the slightest imperfection in the adjustment Adjustment is carried out by sliding the entrance slit holder barrel-assembly in and out of the spectrograph Initial adjustment may be carried out by visual inspection with the detector removed if a suitable spectral source with sharp lines in the visible region is available Once rough focus in the detector plane has been achieved it is necessary to mount the detector and conduct iterative focal adjustments according to detected signal until optimal response has been achieved This adjustment must be carried out whenever the grating is changed as different specifications of grating have variations in their focal lengths of up to 10% However, it was found that the detector could be remounted accurately on the spectrometer This meant that the detector could be removed and replaced without the need to readjust the focal alignment Rotational alignment involves aligning the columns of pixels on the CCD with the spectral line (slit) image of the spectrograph Rotational misalignment may make the spectral line-width appear greater than it actually is when the CCD is binned by column, as the image crosses adjacent columns even though the line-width can be comparable to that of a single pixel For this reason it is necessary to display each CCD row separately, *i e* without binning, to allow proper alignment The software which controls the detector makes it possible to selectively display the signal from any row or collection of rows across the CCD so it is advisable to select five rows which evenly encompass the entire spectral line image

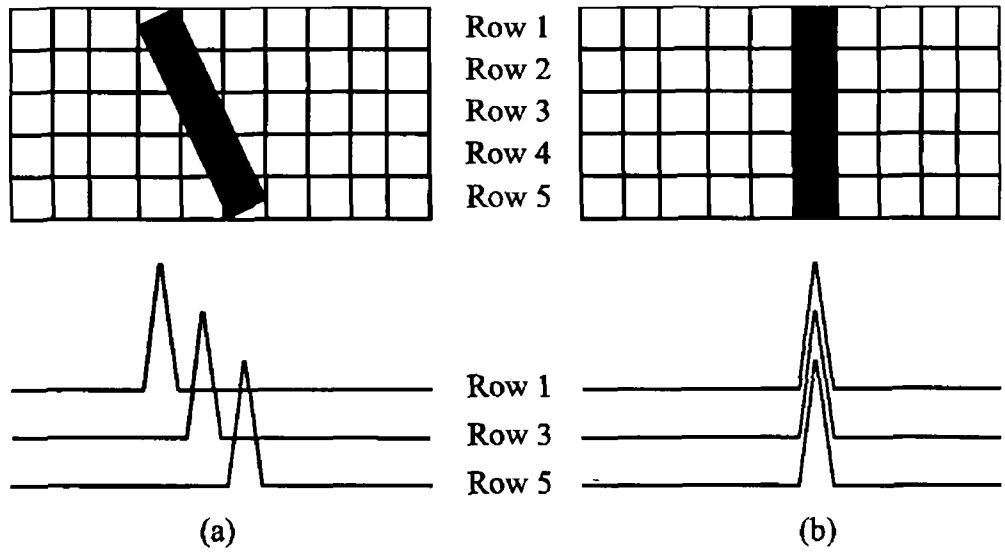

Fig 3 6 Illustration of (a) rotational misalignment where the spectral line skews across the CCD and (b) correct alignment showing the peaks coinciding on separate rows along the CCD

Rotational misalignment should be obvious from this, as peak positions will shift laterally from one row to the next Fig 3 6 illustrates schematically the difference between correct and incorrect rotational alignment The detector can now be rotated relative to the spectrograph as required until the peak positions on each row coincide

More complete instructions for both of these alignment procedures may be found in [3 4] and [3 5]

3 5 2 Frequency calibration

As mentioned in section 3 2 2 there is no *calibration equation* for the 100S/OMA4 combination, that is, there is no known relationship between the movement of the wavelength drive micrometer and the shift of the central wavelength on the CCD For this reason it is necessary to calibrate the system for each new wavelength range

The method of system calibration employed involves the use of wavelength standards based on atomic emission lines The calibration procedure involves placing a suitable light source, usually a low-pressure discharge lamp with emission lines in the region of interest, along the optic axis of the spectrograph and capturing an image of its spectrum with the detector The detector software then allows the known wavelength or frequency values to be assigned to the relevant peaks in the spectrum The software then generates a best-fit equation to describe the relationship between the wavelength units and the pixel positions This equation can be linear, quadratic or cubic as chosen by the user Typically the spectrum is nonlinearly dispersed across the detector, so a polynomial fit is required It is desirable to have as many known peak values as possible

evenly spread across the range when calibrating the system Up to fifteen points may be selected with this software

When the calibration has been completed, the resulting spectrum may be saved to the computer hard disk for future reference If the micrometer reading is noted with this file, the calibration may be retrieved at any time by returning the grating to this position and extracting the calibration coefficients from the saved spectrum Details of the calibration and extraction procedures are given in [3 5]

The calibration of the Raman system is very important as the demands on wavelength accuracy are quite severe and since no standard method exists for calibration of Raman spectrometers, there may be some variation between recorded values and those cited in the literature

The use of wavelength standards offers the advantage of highly accurate calibration points However there are certain disadvantages Firstly, the unavailability of sufficient lines within the region of interest to construct a calibration equation Secondly, the absolute nature of the wavelength standard can be cumbersome if excitation wavelengths are changed since the Raman shift frequency is measured relative to this and does not alter Although the second point was not particularly relevant to the system here it has caused much interest in the development of *Raman shift standards* [3 6], that is, standards based on known Raman shifts from common materials, which may be readily and accurately duplicated Such standards have the advantage of being independent of laser wavelength They are presented in the same manner as the information of interest and cover the region of interest

3 5 3 Frequency response calibration

The procedures for the intensity calibration of Raman spectrometers are much less established than those for frequency calibration There are three issues of interest for intensity calibration Firstly, for quantitative Raman analysis, intensities must be reproducible or be compared to some standard Secondly, if laser wavelength is changed some absolute measure of intensity is required Thirdly, the relative intensities within a spectrum are distorted by the instrument response function It is the last point that is of particular importance here since only one excitation wavelength is in operation The extent of intensity calibration employed is the use of *flat field correction*, that is, the variation in system response with wavelength is corrected to give a normalised or flat profile This essentially involves taking the spectrum of a "white light source", in this case a tungsten lamp, and creating a normalisation function from this which may be

applied to all subsequent spectra Figure 3 7 shows a Raman spectrum of acetone before and after flat field correction

This procedure corrects for relative intensity differences within a spectrum due to the difference in instrument response but in order to make comparisons between spectra other factors must be accounted for Firstly, changes in the laser intensity will have a direct impact on Raman intensity Secondly, sample positioning can have a dramatic

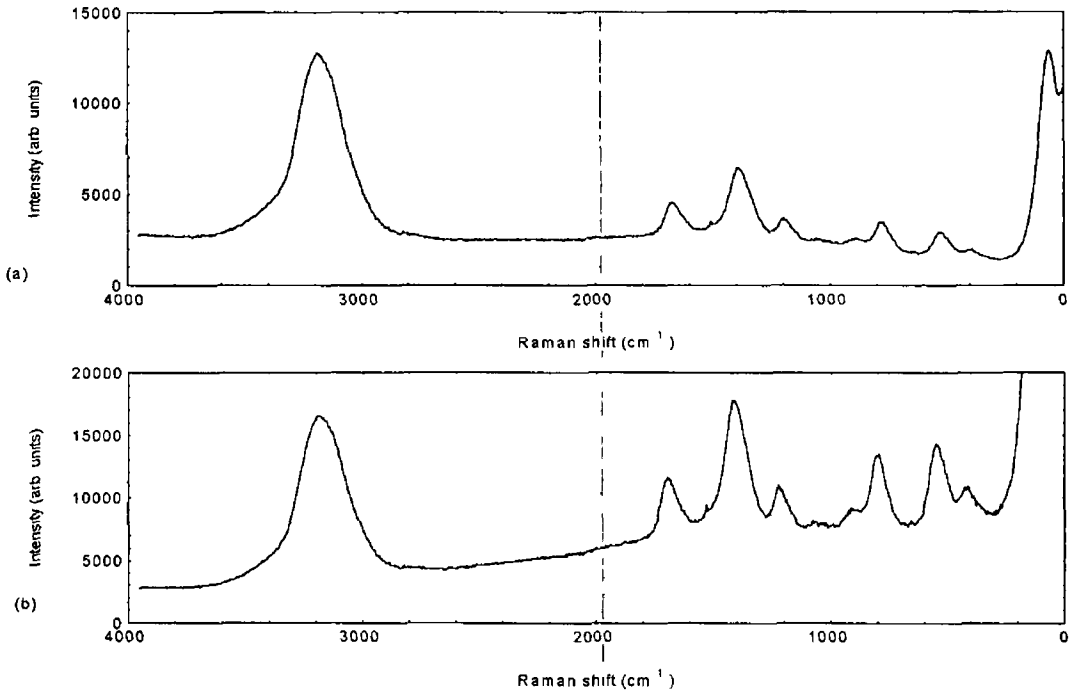

Fig 3 7 Raman spectrum of acetone before (a) and after (b) flat field correction

effect on the observed intensity Although modern laser systems are quite reliably stable in terms of both wavelength and output intensity, the detector system employed here allows for *source compensation*, that is to say any variations in source output can be corrected for An external source monitoring system was designed and developed for this purpose and has obvious benefits when scanning over long time periods as in the case of wafer mapping

3.6 Results

This section contains Raman spectra obtained using the 100S/OMA4 spectrograph/detector combination as described Raman spectra of some common laboratory solvents and a semiconductor sample were obtained

3 6 1 Spectral Resolution

Spectral resolution is an important feature of a Raman spectroscopy system as good resolution is required for useful analysis of Raman spectra However, with a

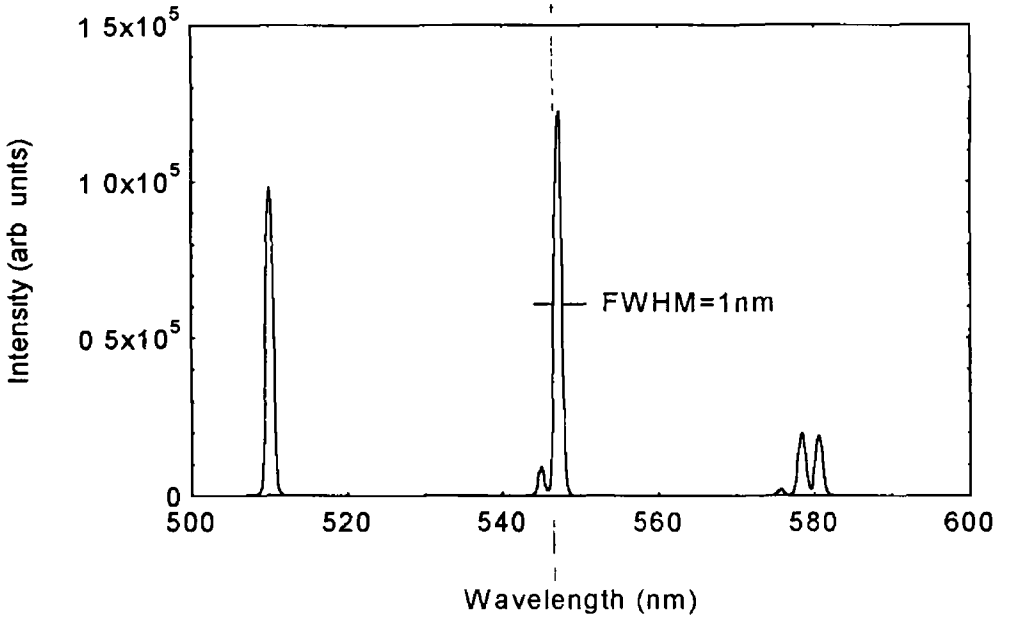

Fig 3 8 Spectrum of Hg/Cd low pressure discharge lamp showing the FWHM of the Hg line at 546 nm and the clearly resolved doublet at 580 nm which is separated by 2 nm

system as described here a trade off between spectral resolution and spectral bandwidth occurs It is quite essential that the wavelength range passed by the spectrograph to the detector must encompass the region of interest for Raman studies, that is 0 to 4000 cm^{-1} The grating used in this spectrograph gave an average linear dispersion across the detector of 8 nm/mm as quoted in its specifications Given that the image zone size of the CCD was 19 5 mm wide this would give a calculated spectral region of 156 nm across the detector corresponding to approximately 4,750 cm^{-1} The observed spectral coverage was from 476-645 nm giving a region of 169 nm corresponding to 5,500 cm^{-1}

The spectral resolution or bandpass was determined by the observation of emission lines from low-pressure discharge lamps These emission lines should experience very little broadening as the lamps operate at relatively low pressure and temperature These lines were therefore assumed to be delta functions for the purpose of determining the instrument response function Figure 3 8 shows spectra of mercury and cadmium obtained with the system, these spectra indicate the FWHM of the spectral line corresponding to the bandpass of the system This may vary slightly across the spectrum due to the nonzero depth of focus of the diffraction grating For a concave grating the depth of focus is approximately twice the product of the slit width and the grating *f/#*, in this case about 220 μm for a 50 μm slit

3 6 2 Spectra

The materials from which spectra were obtained were chosen to test the system and determine its abilities Carbon tetrachloride is a standard benchmark for Raman spectroscopy studies and is chosen as it is a strong Raman scatterer, which allows initial testing and optimization of system setup The Raman bands of CCl_4 give a good indication of system performance close to the exciting line as the primary bands are situated between 200 and 500 cm^{-1} A Raman spectrum of CCl_4 is shown in fig 3 9, which was obtained using the open optic configuration The Raman spectra of CCl_4 taken in the two directions of polarisation are shown in fig 3 10 This demonstrates the ability of the system to obtain useful information about the depolarisation of a vibrational mode

Methanol and acetone were two other solvents that were analysed with this system These were chosen as they are weaker Raman scatterers than CCl_4 and have vibrational bands at larger shift frequencies Figure 3 11 shows Raman spectra of methanol obtained with the open optical arrangement compared to that taken through the optical fibre It can be seen here that there is a notable reduction in the spectral resolution in the case of the optical fibre collection This may be explained by the fact that the optic fibre has a larger effective slit width There would also appear to be a lower S/N ratio for the optical fibre arrangement that may be due to greater stray light within the spectrometer as the fibre slightly overfills the grating This would explain the

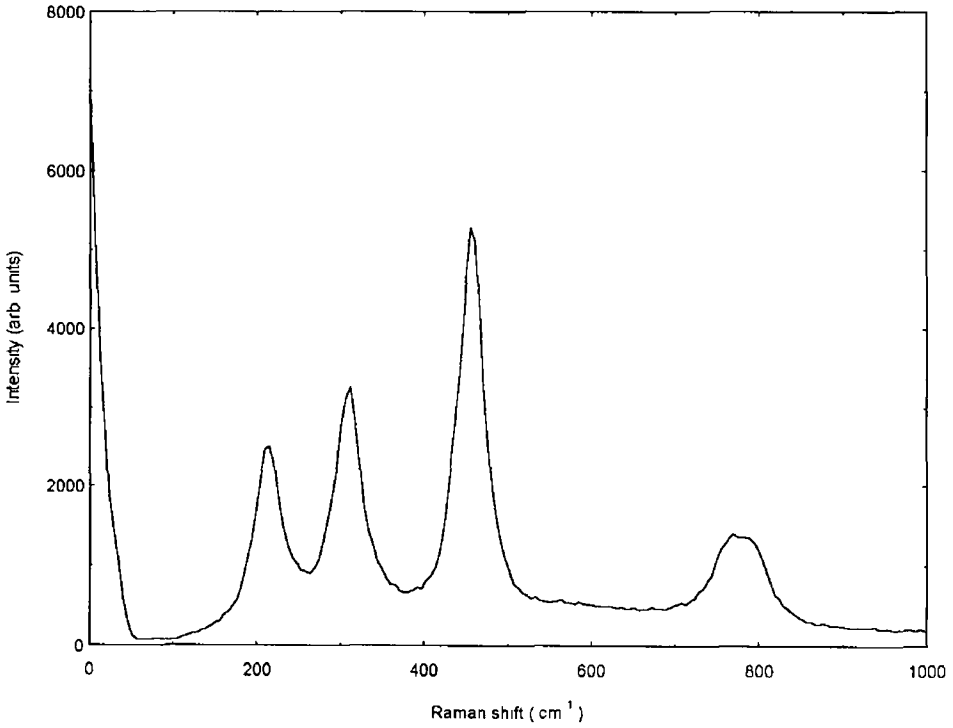

Fig 3 9 Raman spectrum of carbon tetrachloride obtained using the 100S spectrograph and OMA4 CCD combination

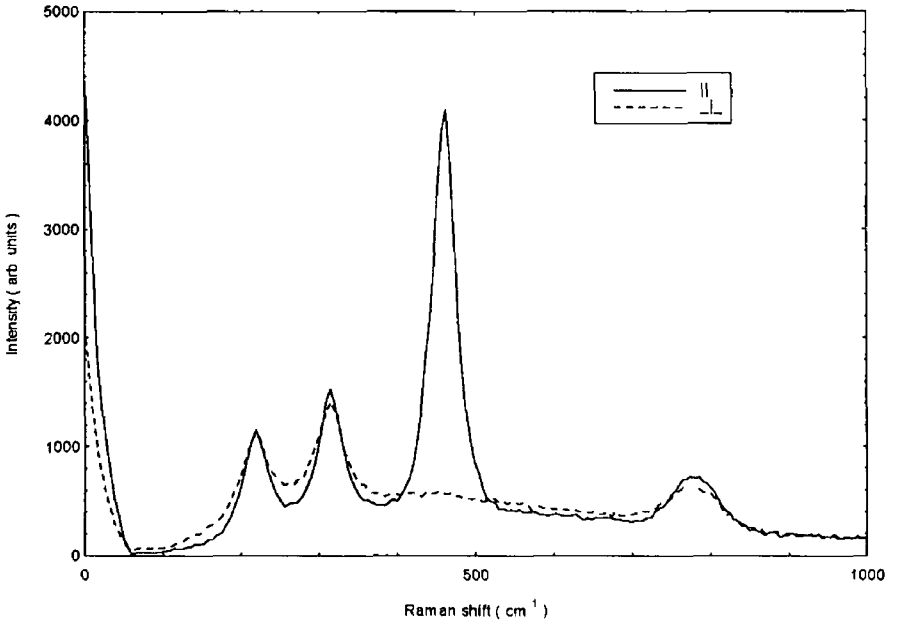

Fig 3 10 Raman spectrum of CCl_4 in two directions of polarisation shows the polarisation of the 459 cm^{-1} vibrational mode

increase of the apparent Rayleigh scatter peak intensity

It is also noticeable that the relative intensity of the Raman bands obtained using the fibre optic collection system are dramatically altered in comparison with the open optics If a correlation between the relative intensities is made, it is noticeable that

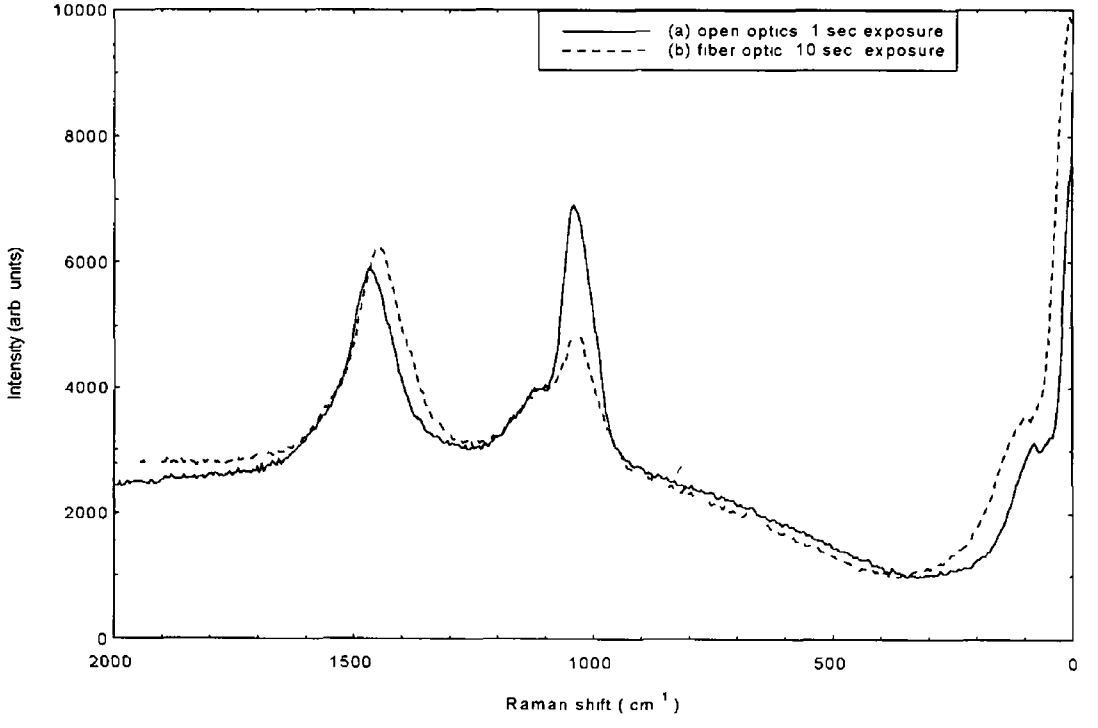

Fig 3 11 Raman spectra of methanol obtained with open optics (a) and with fibre-optic arrangement (b)

Raman band at 1033 cm ^{1} seems to be preferentially reduced in intensity compared with the band at 1490 cm ^{1} in the fibre optic collection situation The possible reasons for this could include a local absorption band in the optical fibre at this wavelength However this would seem to be ruled out by examination of the flat field response of the system with the fibre in place which shows no apparent variations in intensity in this region of the spectrum Another possibility that is considered is the polarisation of the Raman band at 1033 cm ^{1}, which could be affected by polarisation discrimination through the fibre This would explain the reduction in intensity of one line with respect to the other However there is no known polarisation of this band The only remaining explanation for this reduction in intensity of the band at lower wavenumber shift is that the angle of the notch filter may have changed slightly between experiments The effect of a very small alteration of the filter angle on the resulting spectrum can be dramatic as shown in fig 3 12 adapted from reference [3 1] The change of filter angle affects those spectral features closest to the notch wavelength most, which is as observed in fig 3 11 The order of magnitude difference in the exposure times used to yield comparable intensities for both methods would seem to indicate considerable losses in the fibre collection These losses would include absorption by the fibre and reflection losses at the entry

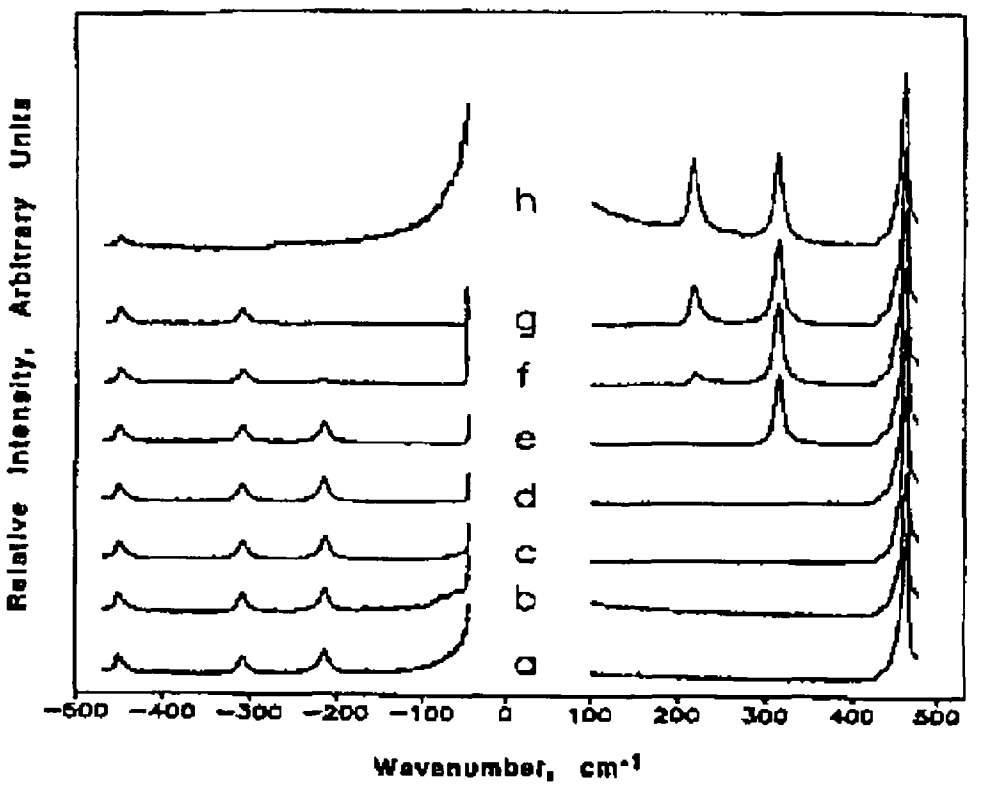

Fig 3 12 Raman spectrum of CCl_4 as a function of holographic notch filter angle. (a) 0^{0},(b) 1^{0}, (c) 4^{0},(d) 7^{0},(e) 10^{0},(f) 12 5^{0},(g) 13^{0},(h) 18^{0} Adapted from reference [3 1]

face The scale of the losses would appear to be a great deal larger than theoretically indicated given the quoted transmission value for the fibre The shift of the 1490 cm^{-1} Raman band is smaller for the fibre optic collection by approximately 10 cm^{-1} As this difference is only manifest at higher shifts it would seem to indicate a deviation between the calibrations for the open optic and fibre optic systems This deviation is within the limit of resolution of the system

The final solvent which was examined was toluene, which was chosen as it has a number of very sharp Raman bands Two of these bands are close together in the spectrum with a separation of less than 30 cm^{-1} This makes toluene suitable as an indicator of spectral resolution in practical terms Figure 3 13 shows a Raman spectrum of toluene obtained with the compact Raman system compared with a similar spectrum taken using a high resolution system It can be seen from this that although the two peaks at 1000 cm^{-1} and 1029 cm^{-1} are evident in the open optics spectrum (bottom) they are not clearly resolved as in the upper spectrum The peaks in the region of 800 cm^{-1}

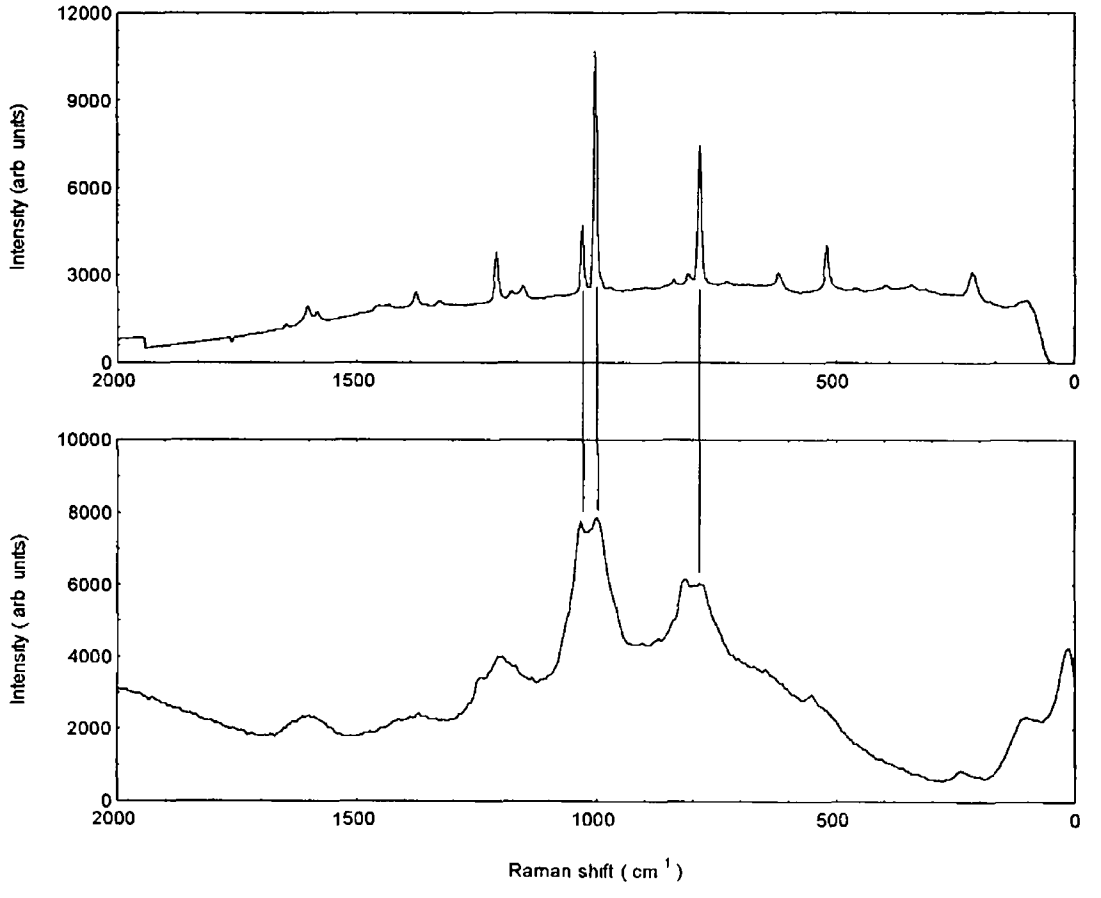

Fig 3 13 Raman spectrum of toluene obtained using an open optic configuration (bottom) compared with a spectrum obtained on a high-resolution commercial system (top) The Raman bands at 1000 cm^{-1} and 1027 cm^{-1} show the limited resolution of the compact system

are quite different in appearance in the bottom spectrum The peak at lower wavenumber shift from the upper spectrum seems to be greatly reduced in comparison to the peak at higher wavenumber shift This may again be attributed to the angle of the notch filter These peaks are superimposed on a fluoresence background, which may also contribute to the appearance of the spectrum This fluoresence was not a factor in the upper spectrum as it was obtained using 632 nm excitation compared to 514 5 nm for the bottom spectrum

Silicon was also examined using the compact system In this case the backscattering geometry was employed and a second holographic notch filter (courtesy of Dr Ger O'Connor, UCG) was used in conjunction with the existing filter This was found to be necessary due to the very low Raman efficency of Si and its high Rayleigh scattering Thus long exposure times were necessary to collect a sufficient signal and the second filter was vital to reduce the level of scattered laser light entering the spectrograph Reducing the scattered laser light was critical to avoid saturation of the detector and to minimise stray light within the spectrograph

Fig 3 14 shows a spectrum of Si obtained with this arrangement The exposure time required to obtain this signal was 60 seconds which shows the weakness of the Raman effect in silicon The ability to collect useable spectra from weakly scattering

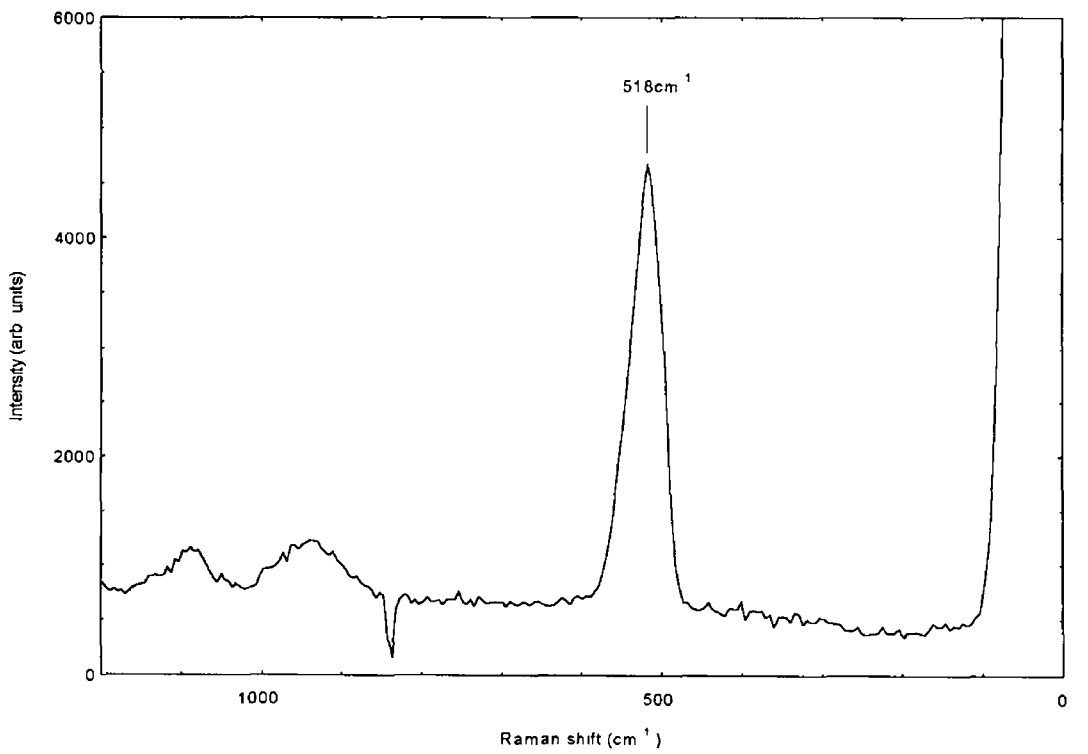

Fig 3 14 Raman spectrum of silicon obtained using the compact Raman system employing a backscattering geometry

solids is shown by this and in particular the ability to analyse semiconductor materials is realised The Si peak was found to be at a Raman shift of 518 cm^{-1} which compares very well with results obtained on a commercial system for the same sample The normal shift position for this peak, which corresponds to the zone-centre TO phonon in Si is quoted as 519 cm^{-1} [3 7]

3.7 Conclusion

This chapter describes the successful implementation and operation of the compact Raman system The tests carried out on the system are outlined and the results of analysis carried out on a number of samples are presented The next chapter outlines a second system implemented for higher spectral resolution analysis, which is complementary to the compact system

Chapter 4

High resolution system

4.1 Introduction

This chapter describes the development of a high resolution Raman spectroscopy system This was motivated by the limitations of the compact system described in the previous chapter in regard to high spectral resolution analysis

The components used in the system are described and the design of the system is outlined Characterisation tests were run on the system and a selection of samples was examined using the system The results of these tests and spectra obtained are presented here

4.2 System components

This section contains a brief description of components employed in the system The excitation source, detector and filter used were the same as used with the compact Raman system and are described in sections 3 2 1, 3 2 3 and 3 2 4 respectively

4 2 1 Spectrometer

The spectrometer used for this high-resolution system was a SPEX model 1704 spectrometer, illustrated schematically in fig 4 1 This is a 1m focal length spectrometer, which employs two concave mirrors of 100 mm diameter and a plane diffraction grating in a Czerny-Turner configuration The grating used for this work was a holographic plane diffraction grating with 300 lines/mm blazed at 2 μm This spectrometer was equipped with adjustable entrance and exit slits For working with the CCD detector system, the exit slits were removed and a detector mount was designed and fabricated to couple the spectrometer and detector The SPEX 1704 has a computer controlled grating drive assembly, which allows rapid and reproducible positioning of the grating at a "center wavelength" value The CCD detector was mounted such that the center of the array was positioned on the optic axis of the spectrometer and the array surface was in the focal plane of the spectrometer at this point It was expected that the focal plane of the exit mirror would be curved however it was found that the radius of curvature of the focal plane for the 1 m focal length mirror was sufficiently large to make focussing errors at the CCD surface negligible This was demonstrated by moving a spectral line across the CCD by rotation of the grating It was noted that the line width

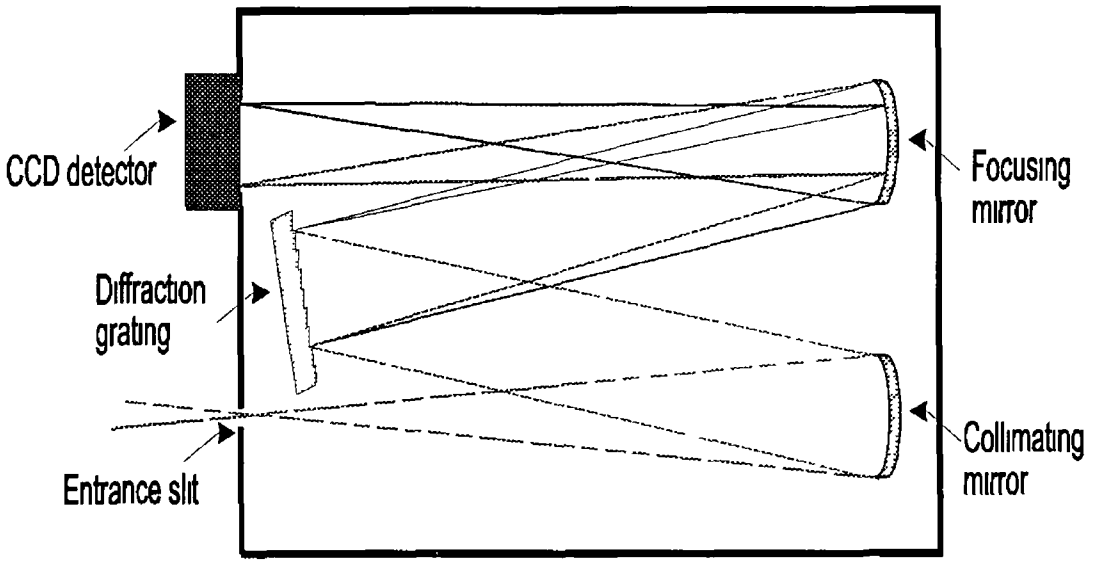

Fig 4 1 Schematic diagram of the SPEX 1704 spectrometer fitted with a CCD detector in place of the exit slit

of this spectral line did not increase as the spectral line moved toward either side of the detector

4.3 System configuration

The optical set-up employed for this high-resolution system was similar to that described for the open optics configuration used with the compact system Collection of the scattered light was performed using the *f/1* plano-convex lens as described in section 3 4 1 and again the holographic notch filter was employed as shown in fig 3 4 In this case however the *f/2 5* delivery lens used for the compact system was replaced by an *f/10* lens in order to allow *f/#* matching to the spectrometer This arrangement magnifies the image of the sampled area by a factor of 10 Following the calculations mentioned in section 3 3 1 in regard to the dimensions of the focal cylinder of the exciting beam it can be seen that the resultant image size at the entrance slit of the spectrometer will be of the order of 150 μm The entrance slits of the SPEX 1704 are adjustable in both height and width and so could be set to encompass the image of the sample It was found however that slit widths of the order of 150 μm were not practical as this resulted in a reduction of the system resolution The slit width chosen is determined by the trade off which occurs between the need to allow maximum flux into the spectrometer while not overfilling the optics and maintaining a sufficiently small bandpass i e maintaining instrumental resolution The best compromise for the entrance slit width was found to

be 100 μm As the irradiance is low with Raman scattering it is vital to maximise the throughput of the spectrometer to achieve a good signal to noise ratio

4.4 Experimental Procedures

This section details procedures relevant to the operation of the system and the preparation of the system before use

4.4.1 Spectrometer Alignment

When a new grating is installed in the SPEX spectrometer, it is usually necessary to perform an alignment of the spectrometer Small misalignments may be corrected for by adjustment of the grating mount and as any adjustment of the mirrors will affect all aspects of the spectrometer alignment, these should only be adjusted when performing a complete alignment of the system

Initially the instrument should be leveled by adjustment of the leg length while monitoring the position of the bubble of the internal spirit level fitted in the spectrometer The entrance slit width and height should be set and the recommended settings are 2 mm for both dimensions [4 1] Now a laser must be mounted on the optical axis of the spectrometer A He-Ne gas laser is suitable for this procedure and an alignment kit may be purchased which contains such a laser and the necessary mounting parts and target masks and fixtures for the mirrors and gratings As this kit was not available, the requisite parts were improvised A He-Ne laser was mounted on an optical rail and placed along the optical axis to illuminate the spectrometer entrance slit The inspection covers on the top of the spectrometer were removed to monitor the light path through the system A target for the collimating (entrance) mirror was fashioned by stretching an elastic band over the four mounting screw heads to have it crossover at the center of the mirror This arrangement proved to serve as an adequate target for centering the laser beam on the first mirror, this procedure ensures that the laser is positioned on the optical axis When this procedure has been successfully completed, the target may be removed from the mirror At this point, the grating should be removed and a fixture inserted in its place, which has a target hole to center the beam at the grating Again as this part was not available, the centering procedure was improvised with the grating in place by using a mask over the grating The grating was scanned to 0 Å to position the grating parallel to the end plate of the spectrometer In this case as there was no gross misalignment of the system it was found that no adjustment of the collimating mirror was necessary to locate the laser beam at the center of the grating

The mask was removed from the grating and the improvised target was fitted to the focussing (exit) mirror The reflected laser beam was aimed at the center of this mirror by moving the grating up and down and from side to side by adjustment of the appropriate screws on the grating mount, see [4 1] for details When this procedure was completed the target was removed from the mirror and the position of the laser beam at the exit slit was examined The focussing mirror could be adjusted to aim the laser beam at the exit slit but again no adjustment of the mirror was necessary in this case The next step in the alignment procedure was to ensure that vertical alignment at the exit slit is maintained at all wavelengths This was achieved by a procedure termed "rocking the grating" The position of the laser at the exit was noted with the grating at 12656 Å, which is the second order of the 6328 Å line of the He-Ne laser and was centered by adjustment of the cam located at the bottom left of the grating mount When this was achieved, the cam was prevented from rotating by tightening the locking screw The grating was then scanned to 0 Å and the position at the slit was checked again and re-centered as required by adjustment of the screw at the top-front of the grating mount This procedure was repeated until the spectrum was satisfactorily centered at both low and high wavelengths

At this point, the exit slits were removed and the CCD detector was mounted onto the spectrometer This allowed the positioning of the spectrum at the detector plane to be checked The laser was replaced by a sodium lamp and the grating was set to 11780 Å (5890 Å in second order) The shutter on the entrance slit was set in the center position and it was confirmed that the resultant spectrum was imaged on the center portion of the CCD This was also checked for different orders to ensure that the rocking of the grating was properly set The entrance slit was set to 30 μm × 0 2 cm and the spectrum of the sodium doublet was captured with the CCD displaying 11 equidistant rows across the height of the detector, shown in fig 4 2 This was performed to ensure the rotational alignment of the spectrograph/detector combination as described previously in section 3 5 1 The peak separation of the sodium doublet also served as an indication of the linear dispersion across the detector This is discussed in section 4 5 1 When the spectrum was imaged in this way it also showed the intensity distribution across the detector which allowed the detected intensity to be maximised, that is, it ensured that the slit height matched to the height of the detector This was important due to the trade off between the benefit of increasing the slit height to increase the flux reaching the detector and the subsequent increase in stray light

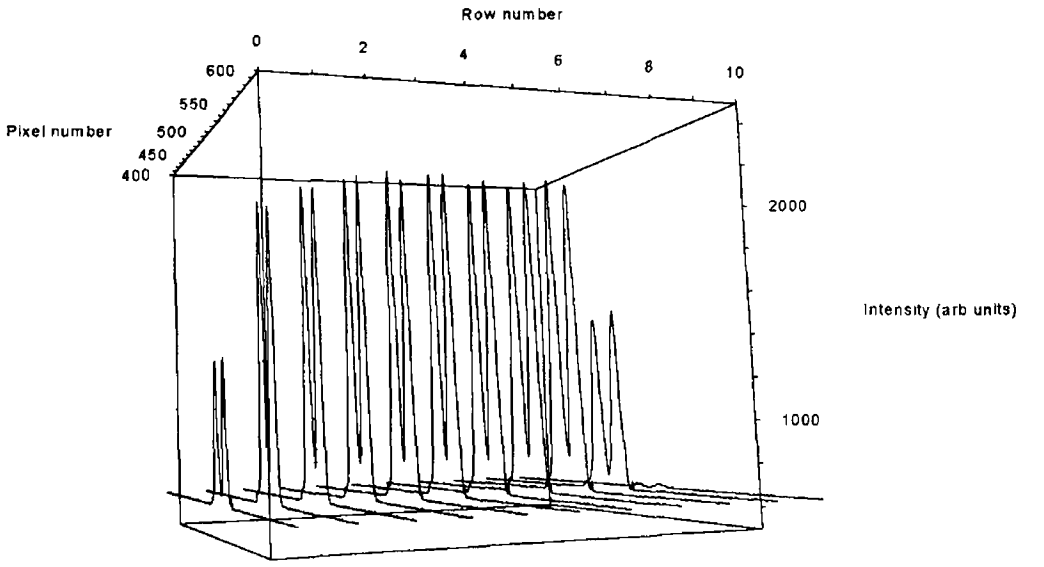

Fig 4 2 Three-dimensional graph showing the image of the sodium doublet captured across eleven rows of the CCD detector, which indicates the intensity distribution

4 4 2 Frequency Calibration

With multichannel detection being employed on the SPEX spectrometer, the instrument behaved as a spectrograph In this mode of operation the counter reading for the spectrometer, which corresponds to the wavelength value at the exit slit, gives the *center wavelength* of the spectrograph Here again there was no calibration equation for the combination of the OMA4 and SPEX 1704 The center wavelength could be determined by the grating drive As the laser wavelength employed was 514 5 nm, it was found that a center wavelength value of 530 nm suitably encompassed the area of interest with the spectrometer operating in second order It was now necessary to calibrate the system for this wavelength range It was found that there was a lack of suitable spectral sources to create an accurate calibration equation for this spectral area At this point, it was decided to create a more complete calibration by encompassing the three elements of spectrometer counter reading, wavelength and pixel number This was achieved by setting the spectrometer counter to a value corresponding to an emission wavelength of the Ar^+ laser, tuning the laser to a range of wavelengths spanning this center wavelength and the spectral range of the CCD/spectrograph By noting the pixel positions of these known wavelengths it was possible to generate a calibration equation for this center wavelength The counter was set to another two emission wavelengths and the procedure was repeated for each In this way, it was hoped that a general

Counter (Å)	Wavelength λ (Å)	Pixel number
4880	4765	123
4880	4880	486
4880	4965	755
4880	5017	920
4965	4880	218
4965	4965	486
4965	5017	652
4965	5145	1000
5017	4880	53
5017	4965	322
5017	5017	488
5017	5145	892

Table 4 1 Calibration data of wavelength and pixel number acquired for three different spectrometer counter values

calibration equation could be created Table 4 1 contains the calibration data acquired in this manner

Figure 4 3 shows a three dimensional graph of counter value vs pixel vs wavelength The surface described by these points is a segment of what may be thought of as a calibration surface that relates all three variables at all points Thus by knowing two variables the third may be found In this case when the counter value and pixel

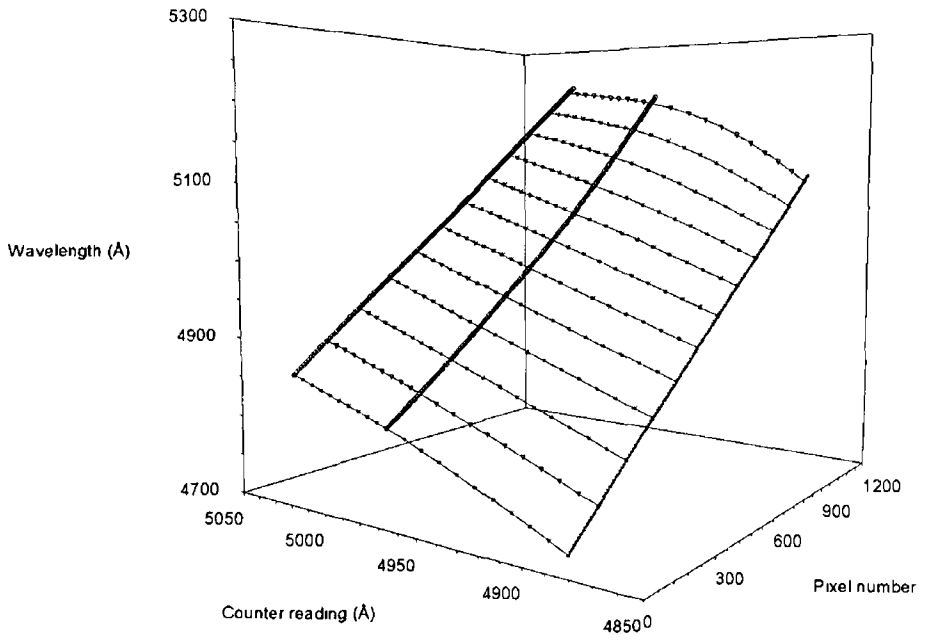

Fig 4 3 Three-dimensional graph of counter value vs wavelength vs pixel number with

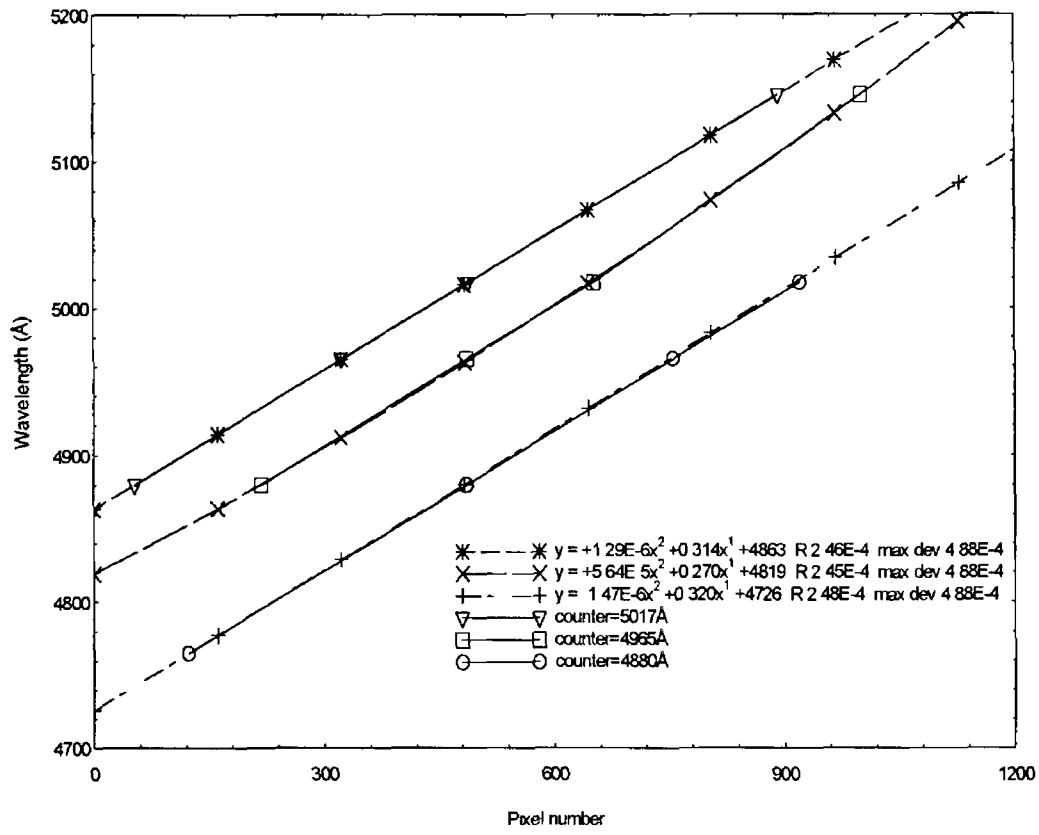

Fig 4 4 Graph of wavelength vs pixel number for the three different counter values showing the calibration equations fitted to each set of data points

position are known the wavelength corresponding to that pixel may be determined The main difficulty with this method of calibration came from the fact that the surface segment generated was quite limited Because of this, extrapolation of this surface would not result in a reliable calibration surface More spectral sources would be required to build up a more complete picture of the behaviour of the system as the grating position is changed The time expenditure required to generate sufficient data to accomplish this task was impractical at this point It was noted that although the terms of the equation linking the wavelength values to pixel numbers did change with increasing counter value, these variations were extremely small, see fig 4 4

On this basis it was decided to apply the equation generated for the counter value which most closely matched that required i e the 501 7 nm counter equation applied to 530 nm counter setting Using this equation, the wavelength values corresponding to the pixel numbers from 1 to 1024 were generated It was found that the center pixel was located at pixel # 490 The difference between this wavelength value and the required center value of 530 nm was calculated and all wavelength values were shifted by this difference to obtain the calibration for the 530 nm counter reading This calibration was applied to all subsequent spectra

4.5 Results

This section contains Raman spectra obtained using the SPEX/OMA4 spectrograph/detector combination as described Raman spectra of some common laboratory solvents were obtained

4 5.1 Spectral Resolution

As mentioned previously spectral resolution is a very important feature of a Raman spectroscopy system and indeed was the motivation for developing this particular system For this spectrograph/detector combination the spectral range encompassed is determined by the linear dispersion across the detector and the detector width The linear dispersion in the case of the Spex spectrometer is determined by the groove density and the order The linear dispersion for the 300 lines/mm grating operating in second order could be calculated from the spectrum of the sodium doublet shown in fig 4 5 The separation between the peaks is 6 4 Å, which corresponds to 20 pixels As each pixel is 19 μm wide this gives a linear separation between the peaks of 0 38 mm thus giving a linear dispersion across the detector of 16 8 Å/mm This figure compares well to value of 16 7 Å/mm quoted in the specifications of the spectrometer Using this figure for average linear dispersion, the spectral range encompassed by the detector is 1165 cm^{-1}, which is equivalent to a range from 0 to −1133 cm^{-1} If the resolution is thought of in terms of the bandpass of the system, it is possible to compute

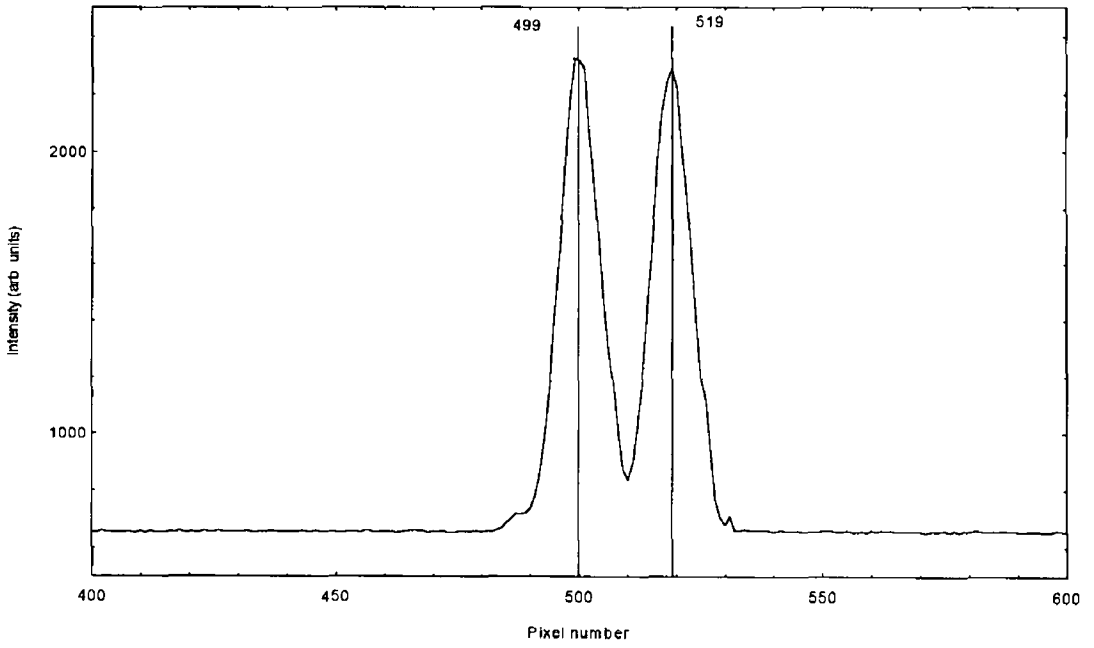

Fig 4 5 Sodium emission spectrum obtained with the high-resolution system showing the pixel separation between the lines at 5889 5 Å and 5895 9 Å

this when the linear dispersion and entrance slit width are known In this case if a slit width of 100 μm is employed the resultant bandpass is approximately 1 7 Å or 6 cm^{-1} at 530 nm This figure only takes into account the dispersion and the entrance slit parameters however the width of each pixel and the number of pixels required to describe each bandpass are also factors in determining the bandpass of the system It is normal to allocate between three and six pixels to determine one bandpass It must also be noted that the image in the exit plane changes in width as a function of wavelength so therefore the FWHM that describes the bandpass also changes A more complete discussion of the use of array detectors with spectrographs and the effects of wavelength changes on pixel position may be found in [4 2]

4 5 2 Spectra

The materials from which spectra were obtained were chosen to test the system and determine its abilities Carbon tetrachloride was chosen as the first substance for analysis to optimise the system setup due to the materials strong Raman bands A Raman spectrum of CCl_4 is shown in fig 4 6, which was obtained with this high-resolution system This spectrum displays far better spectral resolution than that obtained using the compact system (fig 3 9) however the signal to noise ratio is somewhat lower The collection time for the high-resolution spectrum was an order of magnitude greater than that used with the compact system The increase in resolution is

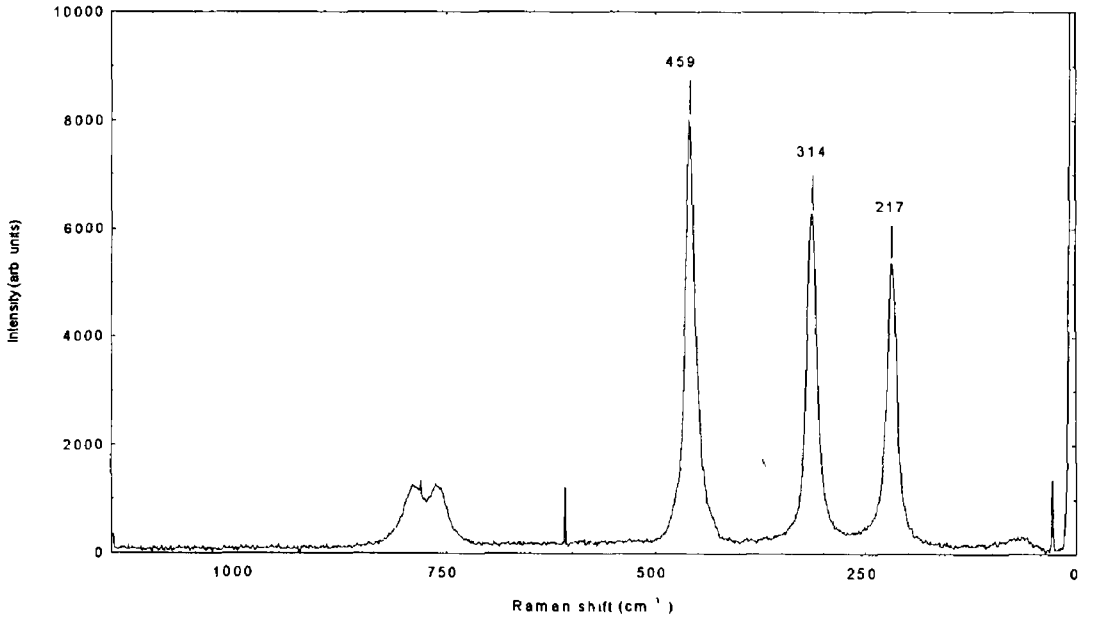

Fig 4 6 Raman spectrum of carbon tetrachloride obtained using the SPEX/OMA4 high-resolution system.

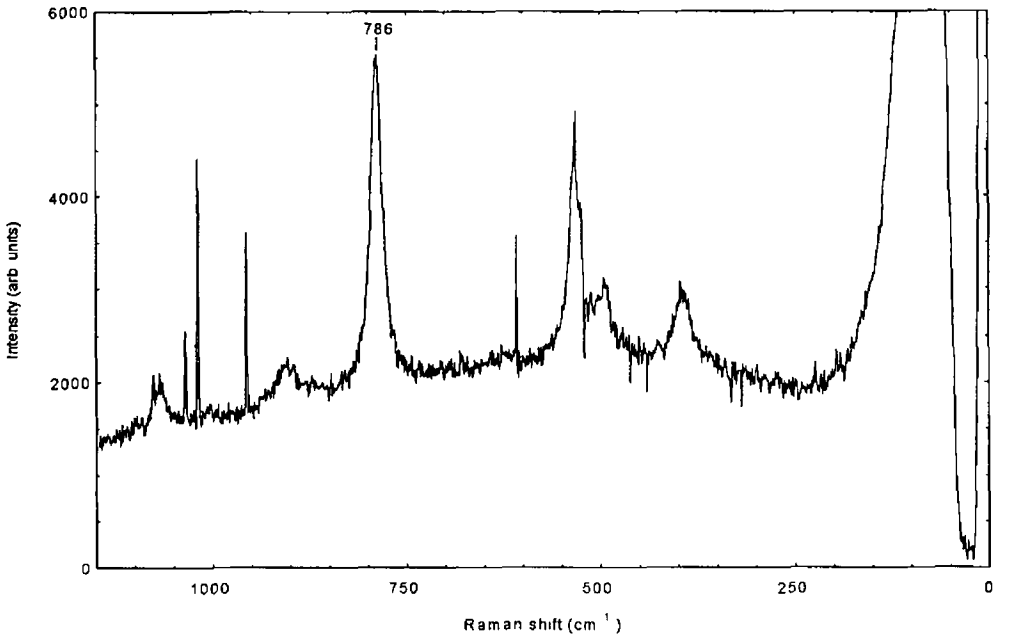

Fig 4 7 Raman spectrum of acetone showing a reduced S/N ratio and an increased number of cosmic ray spikes

noticeable as the doublet with peaks at 760 cm^{-1} and 787 cm^{-1} is discernible The filter cut-off is obvious in this spectrum which indicates a reduction in stray light over the compact system The increase in exposure time has increased the problem of cosmic ray spikes in the spectrum, which can be seen at about 30 cm^{-1} and 600 cm^{-1} in fig 4 6

The next sample to be analysed was acetone which was chosen as it is has weaker Raman bands than CCl_4 Figure 4 7 shows a spectrum of acetone The collection time for this spectrum was 5 minutes, an increase by a factor of 5 from the CCl_4 collection time In this case the signal to noise ratio is noticeably reduced and the problem of cosmic ray spikes is much more prevalent The cut-off band of the notch filter is quite obvious here due to the presence of scattered laser light beyond the edge of the band The main Raman band of acetone is evident at 786 cm^{-1} The increased resolution is again noticeable over the equivalent spectrum obtained with the compact system shown in fig 3 7

The final solvent examined was toluene, which was chosen to test the ability of the system to resolve the closely spaced and very sharp bands in Raman spectrum of this material Fig 4 8 shows a Raman spectrum of toluene obtained with the high-resolution system in a collection time of 5 minutes The improvement in resolution of this system over the compact system, see fig 3 13, is very evident here as the Raman bands at 1004 cm^{-1} and 1030 cm^{-1} are clearly resolved The other Raman bands of toluene are also visible in the spectrum There is an improved signal to noise ratio in this spectrum when compared to the spectrum of acetone obtained with a comparable

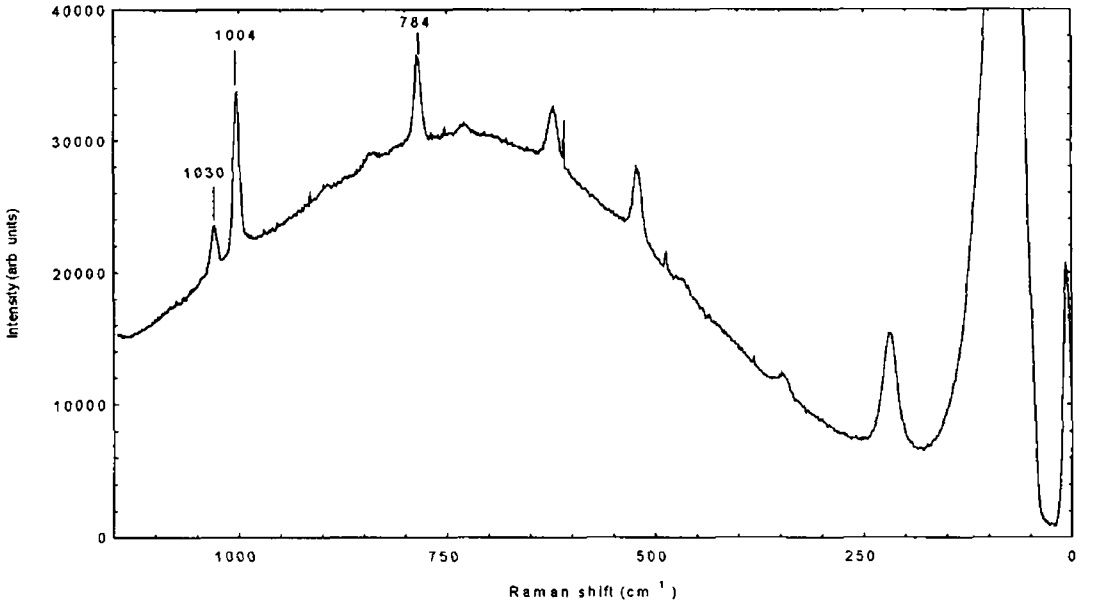

Fig 4 8 Raman spectrum of toluene obtained on the high-resolution system showing the bands at 1004 cm^{-1} and 1030 cm^{-1} to be clearly resolved

exposure time Although they overlap a broad fluoresence peak, all the characteristic Raman peaks of toluene are clearly observable and resolved

In this spectrum, the band of laser scatter beyond the edge of the notch filter is again very noticeable This feature in the spectrum is a major problem in regard to the analysis of materials with low Raman efficiencies This became very noticeable when the analysis of silicon was attempted In this case, the detector was saturated by this laser scatter before the Raman band of silicon could be observed

It should be noted that flat-field correction was not performed for the spectra shown in figs 4 6 to 4 8

4.6 Conclusions

This chapter describes the successful implementation and operation of a high resolution Raman system The tests carried out on the system are outlined and the results of analysis carried out on a number of samples with the system are presented The performance of both systems is discussed in the next chapter The problems encountered are discussed and possible solutions to these problems are outlined

Chapter 5

Conclusion

5 1 Summary

The objective of this project was to design and construct a system to facilitate the analysis and characterisation of materials using Raman spectroscopy as the characterisation technique

In the event two separate systems were built The first system was a highly compact and portable system, which allowed fibre coupling of the collection optics to the spectrograph and could be combined with an existing system for the purpose of mapping semiconductor wafers using Raman scattering The second system was a high-resolution system, which could facilitate more detailed spectral analysis of materials than the compact system

The results displayed in chapters 3 and 4 are indicative of the successful operation of these systems The ability to analyse both solid and liquid samples is demonstrated and the capacity for polarisation analysis of vibrational bands is displayed Both systems were characterised in terms of spectral resolution and the methodology for characterisation of spectral response was demonstrated with the compact system The Raman spectra of common materials obtained with both systems compare very well with results reported previously by other researchers and those obtained using commercial systems

The components vital to the success of these systems were the CCD detector and the holographic notch filter Recent developments in the production of these component parts have made Raman systems, such as the compact system developed here, possible These components are at the cutting edge of the technology, however with both systems developed here, the limiting factor to the system performance was the spectrometer used In the case of the compact system the throughput of the system was excellent, however the spectral resolution was suitable only for the most rudimentary analysis With the motivation of obtaining higher spectral resolution, the second system was developed The high-resolution system was found to provide the necessary improvement in resolution, however, the reduction in system throughput and corresponding increase in collection time and decrease in signal to noise ratio was discouraging Ultimately both systems performed satisfactorily but as with any

prototype system, certain problems existed These are discussed and solutions proposed in the following section

5.2 Suggestions for future work

The Raman systems described here are still at the developmental stage and as such there are certain aspects of both systems that could be improved to increase their capabilities

As mentioned in the previous section, one of the main limiting factors of the systems developed here were the spectrographs employed As Raman spectroscopy deals with such low signal levels, it is imperative to maximise the throughput of the system and it was found that the compact system performed well in this regard due to the fact that it employed a fast (low *f/#*), single element spectrometer The spectral resolution was not really sufficient with this spectrograph, so initially it was proposed to have a more suitable grating designed for use with it American Holographic, the manufacturers of the spectrograph and its gratings, were approached with a view to fabricating a higher dispersion grating for the spectrograph The design engineer found that this was essentially not possible with such a short focal length spectrograph The suggested solution would involve using a spectrograph of at least *f/3 3* In practical terms this would mean building a completely new spectrograph, which was not practical at this time The use of a single element, concave holographic reflection grating, spectrograph offers the best solution to the problem of system throughput with reflection-based technology There is another fundamental problem with spectrograph/CCD based systems which is evident from the high-resolution system, that is, the trade off that occurs between spectral resolution and spectral coverage The compact system developed here offers almost ideal spectral coverage but the high-resolution system can only interrogate approximately one quarter of the requisite spectral area The solution to this problem can only be found by moving to the next generation of grating technology, which is the holographic transmission grating [5 1] This type of grating has two major advantages, firstly it offers higher throughput than a reflection based grating and more importantly it can be multiplexed Multiplexing essentially involves superimposing two holograms on the grating at a slight angle to each other so that two different spectral ranges are dispersed (horizontally) by the grating and are displaced (vertically) from each other This means that imaging two halves of a spectrum on two different portions of the CCD doubles the spectral range

This technology is employed in the latest generation of Raman spectrometers from Kaiser Optical Systems, Inc [5 2]

A major problem encountered while developing these Raman systems was the difficulty of aligning the laser focussing and collection optics As mentioned in section 3 3 1, focussing the excitation beam onto the sample is essential to increase the Raman signal The alignment of the collection optics with a tightly focussed beam involved a great deal of painstaking adjustment to optimise the signal There was also the problem of reproducibility with this arrangement The most straightforward solution to this problem is to employ a confocal arrangement similar to that used in Raman microscopy systems In the confocal system the illumination and collection is carried out by the same lens, this guarantees alignment of the optical system and greatly simplifies signal collection This optical arrangement only allows back scattering collection, which can be restrictive but is convenient for general material analysis The confocal system requires a beamsplitter to steer the laser beam into the lens for excitation and pass the scattered light back to be collected Holographic beamsplitters are ideal for this application, these are essentially holographic notch filters designed to operate at a 45 degree angle This type of beamsplitter has very high reflectivity at the laser beam wavelength on the input and high transmission except at the laser line, which it will attenuate by about one optical density, on the return path [5 3]

It was mentioned in chapter 3 that, for low efficiency Raman scattering materials, the Rayleigh rejection provided by a single notch filter was not sufficient The use of notch filters in series provides a solution to this problem and some commercial systems use as many as three filters in the collection path, which dramatically reduces the Rayleigh scatter entering the spectrometer and thereby reduces any consequential stray light The addition of even a second notch filter to the systems developed here would greatly extend the range of materials that could be analysed

There are certain mechanical improvements that could be made to the system The method of setting the filter angle could be improved as it was seen to be a possible source of difficulty The arrangement employed here allowed the filter to be set to an angle and fixed in position There was no facility to allow accurate, reproducible angular positioning of the filter As shown in fig 3 12 by Yang et al [3 1], changes in angle of the filter by as little as 3 degrees can greatly alter the appearance of resulting spectra This problem could be solved by the addition of a rotation table on which the filter could be mounted to allow minute adjustment and reproducible angular positioning of the filter

The CCD employed in these systems was quite adequate in terms of performance However, more recent generations of this device offer the benefits of a more compact package and the introduction of Peltier cooling systems which can operate with the use of air for heat transfer rather than water, which was required for the CCD system employed here Thus the application of such a device would increase system portability

A certain amount of work was carried out to develop the compact system for it to be used in conjunction with the existing wafer mapping facility Ultimately the success of the combined system relies on some of the additional work described above In particular, the use of a beamsplitter as described is essential, so too is the use of additional notch filters The scale of the collection times required to obtain a Raman signal from materials, such as silicon, with the compact system was discouraging in relation to the use of the system for large area mapping It would be expected that this time-scale could be considerably reduced by the application of the confocal arrangement and the other suggested improvements to the system throughput Until the time required to obtain a useful signal is reduced to less than a second, the use of this system for whole wafer mapping would be impractical The improvements made to the mapping system, as suggested [5 4] are equally applicable to PL mapping and certainly enhance the efficiency of the mapping system for this purpose

5 3 Conclusion

The capabilities of the Raman facilities, developed during the course of this project, were demonstrated by analysis of a variety of materials The complementary nature of the two systems developed was shown and the versatility of the compact system was described in relation to its portability, variability of collection arrangements and adaptability for use with another system to extend its capabilities

These prototype systems provide a useful analytical tool and a sound basis for future research and development

References

Chapter 1

[1 1] Stradling, R A and Klipstein, P C *Growth and Characterisation of Semiconductors* (IOP Publishing, 1990)

[1 2] Perkowitz, S *Optical Characterisation of Semiconductors* (Academic Press, London, 1993)

[1 3] Fauchet, P M "Applied Optical Diagnostics of Semiconductors", *Proceedings of the IEEE*, **80**, pp 420-435 (1992)

[1 4] Chase, B "A New Generation of Raman Instrumentation", *Appl Spectrosc* , **48**, pp 14A-18A (1994)

[1 5] Nakashima, S , Hangyo, M "Characterisation of Semiconductor Materials by Raman Microprobe", *IEEE Journal of Quantum Electronics*, **25**, pp 965-975 (1989)

[1 6] Hayes, W , Loudon, R *Scattering of Light by Crystals* (Wiley, New York, 1978)

[1 7] Raman, C V "A New Class of Spectra due to Secondary Radiation", Ind J Phys , **2**, pp 387-400 (1928)

Raman, C V "A Change of Wavelength in Light Scattering", Nature, **121**, pp 619-620 (1928)

[1 8] Chang, R K , Long, M B "Optical Multichannel Detection", in *Light Scattering in Solids II*, ed by Cardona, M, Guntherodt, G , Topics in Appl Phys , Vol **50**, (Springer, Berlin, Heidelberg 1983) Chap 3, pp 179-205

[1 9] Huang, Y , Yu, P Y "Variable Bandpass Filter with High Rejection Ratio for Raman Scattering", Rev Sci Instrum , **59**, pp 190-191 (1988)

[1 10] Yamamoto, N et al "Practical Use of Easy Raman Spectrometer Equipped with $AgGaSe_2$ Filter and GaAlAs Laser Diode", Jpn J Appl Phys , **32**, Suppl 32-3, pp 123-124 (1993)

[1 11] Carrabba, M M et al "The Utilisation of a Holographic Bragg Diffraction Filter for Rayleigh Line Rejection in Raman Spectroscopy", Appl Spectros , **44**, pp 1558-1561 (1990)

[1 12] Pelletier, M J and Reeder, R C "Characterisation of Holographic Band-Reject Filters Designed for Raman Spectroscopy", Appl Spectros , **45**, pp 765-770 (1991)

[1 13] Delhaye, M and Migeon, M Compt Rend Acad Sci Paris, **262**, pp 702, (1966)

[1 14] Dhamelincourt, P and Wallart, F "Laser Raman Molecular Microprobe (MOLE)", Anal Chem , **51**, pp 414A-421A (1979)

Chapter 2

[2 1] Hayes, W and Loudon, R *Scattering of Light by Crystals* (Wiley, New York, 1978)

[2 2] Stevenson, C L and Vo-Dinh, T in *Modern Techniques in Raman Spectroscopy*, Laserna, J J (Ed), (Wiley, Chichester, 1996) pp 1-38

[2 3] Yu, P Y and Cardona, M *Fundamentals of Semiconductors* (Springer-Verlag, Berlin, 1996)

[2 4] Placzek, G "Rayleigh-Streuung und Raman-Effekt", in *Handbuch der Radiologie*, Marx, E (Ed), (Akademische Verlag, Leipzig, 1934), **V1,2**, p 205

[2 5] Ferraro, J R and Nakamoto, K *Introductory Raman Spectroscopy* (Academic Press, London, 1994)

[2 6] Fleishmann, M et al Chem Phys Lett , **26**, pp 163 (1974)

[2 7] Zahn, D R T *"In situ* Raman Spectroscopy of Semiconductor surfaces and Interfaces", Phys Stat Sol (A), **152**, pp 179-189 (1995)

[2 8] Saint-Cricq, N et al "Raman Determination of the Composition in Semiconductor Ternary Solid Solutions", J Appl Phys , **61**, pp 1206-1208 (1987)

[2 9] Shen, H and Pollak, F H "Raman Scattering Determination of Carrier Concentration and Surface Space Charge Layer in <100> n-GaAs", *Spectroscopic Characterisation Techniques for Semiconductor Technology II*, Proceedings of the SPIE, **524**, pp 145-151 (1985)

[2 10] Nakashima, S , Hangyo, M "Characterisation of Semiconductor Materials by Raman Microprobe", *IEEE Journal of Quantum Electronics*, **25**, pp 965-975 (1989)

[2 11] Brueck, S R J et al "Raman Measurements of Stress in Silicon-on-Sapphire Device Structures", Appl Phys Lett , **40**, pp 895-898 (1982)

[2 12] Hopkins, J B et al "Raman Microprobe Determination of Local Crystal Orientation in Laser Annealed Silicon", Appl Phys Lett , **44**, pp 535-537 (1984)

[2 13] Kolb, G and Salbert, Th "Raman-microprobe Study of Stress and Crystal Orientation in Laser-crystallized Silicon", J Appl Phys , **69**, pp 3387-3389 (1991)

[2 14] Menendez, J et al "Raman Spectroscopy as a Diagnostic Technique for Semiconductor Materials and Devices", *Proc of the Symposium on Diagnostic Techniques for Semiconductors (Oct 1994, Miami, FL, USA)*, The Electrochemical Society Proceedings, **94**, pp 217-227 (1994)

[2 15] Muggli, R Z and Anderson, M E "Raman Micro-Analysis of Integrated Circuit Contamination", Solid State Technol , **4**, pp 287-291 (1985)

[2 16] Kobayashi, H et al "Study of Si Etch Rate in Various Compositions of SC1 Solution", Jpn J Appl Phys , **32**, pp L45-L47 (1993)

[2 17] Yarwood, J "The use of Infrared and Raman Spectroscopy to Study Interfaces", Spectroscopy Europe, **8**, pp 8-17 (1996)

[2 18] Lai, E P C and Ghaziaskar, H S "Noninvasive Spectroscopic Detection of Bulk Polymerization by Stimulated Raman Scattering", Appl Spectros , **48**, pp 1011-1014 (1994)

[2 19] Dhamelincourt, P and Wallart, F "Laser Raman Molecular Microprobe (MOLE)", Anal Chem , **51**, pp 414A-421A (1979)

[2 20] Greenler, R G and Slager, T L Spectrochim Acta, **29A**, pp 193 (1973)

[2 21] Levy, Y , Imbert, C , Ciperiani, J Racine, S , Dupeyrat, R Optics Comm , **11**, pp 66 (1974)

[2 22] Turrell, G "Raman Sampling", in *Practical Raman Spectroscopy*, Gardner, D J and Graves, P (Eds), (Springer-Verlag, Berlin, 1989) pp 13-54

[2 23] Nemanich, R J et al "Raman Scattering Characterisation of Titanium Silicide Formation", IEEE Journal of Quantum Electron , **QE25**, pp 997-1002 (1989)

[2 24] Tsang, J C and Iyer, S S "Raman Spectroscopy and the Characterisation of Buried Semiconductor Layers", IEEE Journal of Quantum Electron , **QE25**, pp 1008-1011 (1989)

[2 25] M^{c}Glynn, E (Dublin City University), *Private Communication*

[2 26] Knight, D S and White, W B "Characterisation of diamond films by Raman spectroscopy", J Mater Res , **4**, pp 385-393 (1989)

[2 27] Louden, J D "Raman Microscopy" in *Practical Raman Spectroscopy*, Gardner, D J and Graves, P (Eds), (Springer-Verlag, Berlin,1989) pp 119-150

[2 28] Huong, P V "New Possibilities of Raman Micro-Spectroscopy", Vibr Spectrosc , **11**, pp 17-28 (1996)

[2 29] Owen, H et al "New Spectroscopic Instrument based on Volume Holographic Optical Elements", Proceedings of the SPIE, **2406**, pp 260-267 (1995)

Chapter 3

[3 1] Yang, B et al "Holographic Notch Filter for Low-Wavenumber Stokes and Anti-Stokes Raman Spectroscopy", Appl Spectros , **45**, pp 1533-1536 (1991)

[3 2] Owen, H "Holographic Optical Components for Laser Spectroscopy Applications", Proceedings of the SPIE, **1732**, pp 324-332 (1992)

[3 3] White, S M Sc Thesis, Dublin City University (1996)

[3 4] American Holographic model 100S spectrometer users manual

[3 5] EG&G Princeton Applied Research, OMA Spec 4000 users manual

[3 6] McCreery, R in *Modern Techniques in Raman Spectroscopy*, Laserna, J J (Ed), (John Wiley and Sons, Chicester) 1996, pp 62

[3 7] Yu, P Y and Cardona, M *Fundamentals of Semiconductors*, (Springer-Verlag, Berlin, 1996)

Chapter 4

[4 1] *SPEX 1704 spectrometer users manual*, Instruments SA

[4 2] Lerner, J M and Thevenon, A *The Optics of Spectroscopy A Tutorial V2 0*, Jobin Yvon Optical Systems/ Instruments SA

Chapter 5

[5 1] Vila et al "Design of Aberration-Balanced High-Efficiency Focusing Holographic Gratings", Appl Opt , **27**, pp 3013-3019 (1988)

[5 2] Owen, H et al "New Spectroscopic Instrument based on Volume Holographic Optical Elements", Proceedings of the SPIE, **2406**, pp 260-267 (1995)

[5 3] Owen, H "Holographic Optical Components for Laser Spectroscopy Applications", Proceedings of the SPIE, **1732**, pp 324-332 (1992)

[5 4] White, S M Sc Thesis, Dublin City University (1996)

Appendix A

Computer Code

The following computer code is written in a customised Pascal based language It was found that there were certain limitations imposed by the fact that this language did not have all the features of standard Pascal In particular, the communication abilities of this language were very basic, however, this program demonstrates how the OMA-SPEC-4000 software can communicate with an RS232 controlled instrument using the macro commands, which directly access the IBM PC memory

This program combines the control of the CCD, and the acquisition of data from it, with the control of the x-y table via the NF90 controller This allows the entire mapping system to be controlled from one computer and means that the mapping procedure is completely syncronised and optimised

NOTE {All text enclosed in brackets, as here, denotes comments which do not have any effect in the program}

```
{Program code begins here, program name is defined}
PROGRAM CCDXY3,
{All variables used in the program are defined}
VAR
  t, com_port, err                integer,
  port_address,snd_byte           word,
  rsp_byte  rs_byte               word
  check, count1, count2           integer,
  s, p , c ,k ,l ,m               integer,
  out_file                        text,
  comp                            real,
  a1                              array[1 1000] of long_integer  {Peak intensities of line 1}
  b1                              array[1 1000] of long_integer, {Peak positions of line 1}
  a2                              array[1 1000] of long_integer  {Peak intensities of line 2}
  b2                              array[1 1000] of long_integer, {Peak positions of line 2}
  a3                              array[1 1000] of long_integer, {Peak intensities of line 3}
  b3                              array[1 1000] of long_integer, {Peak positions of line 3}
  c1                              array[1 1000] of real,         {Source compensation values}
  dat_pt_num, numlines            integer,
  prompt_text                     string,
  range, center                   integer,
  center1, center2, center3       integer,
  range1, range2, range3          integer,
```

```
  r, d, e, f                    integer,
  curve                         integer,
  press                         boolean,
  keyhit                        word,
  namefile1, namefile2          string,

{All procedures used in the program are contained in the following section}
{The following procedure defines a long delay by looping 3000 times}
procedure ldelay,
begin
 for t =1 to 3000 do
 begin
 end,
end,

{The following procedure defines a standard delay by looping 500 times}
procedure delay,
begin
 for t =1 to 500 do
 begin
 end,
end,

{following procedure defines a BUFFER delay by looping 1000 times}
procedure bdelay,
begin
 for t =1 to 1000 do
 begin
 end,
end,

{The following procedure defines a short delay, used to ensure that the RS232 interface can keep up with
the speed at which the macro writes to the RS232 port}
procedure sdelay,
begin
 for t = 1 to 100 do
 begin
 end,
end,
```

```
{The following procedure handles error conditions, gives the user an error message and sets the error flag
accordingly}
procedure error,
begin
 writeln(),
 buflen =42,
 write('error  program terminated'),
 delay(),
 err =1,
end,

{The following procedure sends the individual characters via the COM port to the RS232 instrument}
procedure transmit,
begin
 s_port(port_address,snd_byte),   {send the character}
 sdelay(),
 rs_byte = g_port(port_address), {clear the input buffer}
end,
{The following procedure writes text messages to the screen}
procedure write_text,
begin
 buflen  = strlen(prompt_text),
 writeln(),
 write(prompt_text),
end,

{The following procedure sets the position of the lines to search for in the spectrum  The user is prompted
to enter a center wavelength and a ± wavelength range (in terms of pixels) to define the area in the
spectrum in which to find the peak intensity an corresponding wavelength for up to three different
spectral lines}
procedure set_lines,
begin
prompt_text  = 'Enter the number of lines to monitor (1-3) -->'
write_text(),
read(numlines),
for r =1 to numlines do
 begin
  if r = 1 then
  begin
   prompt_text  = 'Enter in the first center wavelength (pixels) -->',
   write_text()
   read(center1),
```

```
 writeln(),
 prompt_text = 'Enter the λ range about center (pixels)-->',
 write_text(),
 read(range1),
 writeln(),
end,
if r = 2 then
begin
 prompt_text = 'Enter in the second center wavelength (pixels) -->'
 write_text(),
 read(center2),
 writeln(),
 prompt_text = 'Enter the λ range about center (pixels)-->',
 write_text(),
 read(range2),
 writeln(),
end,
if r = 3 then
begin
 prompt_text = 'Enter in the third center wavelength (pixels) -->',
 write_text(),
 read(center3),
 writeln(),
 prompt_text = 'Enter the λ range about center (pixels)-->',
 write_text(),
 read(range3),
 writeln(),
end,
end,
end,
```

{The following procedure finds the peak positions within the given ranges and records both the peak intensity and position}

```
procedure find_peaks,
begin
buflen = 20,
f = 1,
f = g_curve_set_index('lastlive',',0),          {find live data}
cs[f] display = 0,                              {don't plot curve to screen}
for r = 1 to numlines do
begin
 max1 = 0,
```

```
if r = 1 then
begin
center  = center1,
range  = range1,
end,
if r = 2 then
begin
center  = center2,
range  = range2,
end,
if r = 3 then
begin
center  = center3,
range  = range3,
end,
for s  = -range to range do          {Searches through the defined range for the max value}
 begin
  k  = center + s,
  if cs[f] [curve] y[k] > max1 then
   begin
    max1   = cs[f] [curve] y[k]
    c  = k,
   end,
  end,
if r=1 then                          {Writes the max value and position to the appropriate }
begin                                {position in the respective arrays                    }
  a1[count1]  = max1,
  b1[count1]  = cs[f] [curve] x[c],
end,
if r=2 then
begin
  a2[count1]  = max1,
  b2[count1]  = cs[f] [curve] x[c],
end,
if r=3 then
begin
  a3[count1]  = max1,
  b3[count1]  = cs[f] [curve] x[c],
end,
end,
end,
```

```
{This procedure saves the data contained in the arrays to file, the user is allowed to enter the filename}
procedure save_to_file,
begin
 dat_pt_num =count1,
  prompt_text  = 'Enter filename to save scan data -->',
  write_text(),
  read(namefile1),                    {Records the filename entered by user}
  writeln(),
 assign(out_file,namefile1),          {Set the name of the file in which to save data}
 buflen  = 10,
{The data contained in arrays is written to file, there are two columns (peak intensity and position) for
each spectral feature analysed and one column containing the source compensation value, each row
corresponds to a different point of the map}
 if numlines=1 then
  begin
   for p  = 0 to dat_pt_num-1 do
    writeln(out_file, a1[p], b1[p], c1[p]),
  end,
 if numlines=2 then
  begin
   for p  = 0 to dat_pt_num-1 do
    writeln(out_file, a1[p], b1[p], a2[p], b2[p], c1[p]),
  end,
 if numlines=3 then
  begin
   for p  = 0 to dat_pt_num-1 do
    writeln(out_file, a1[p], b1[p], a2[p], b2[p], a3[p], b3[p], c1[p]),
  end,
 close(out_file),
end,

{The following procedure sets the CCD parameters, performs a scan and records the source compensation
value}
procedure scan,
begin
 ds_da(1),                    {Set D A  mode to 1 - acquire a live curveset and stop}
 ds_et(0 01),                 {Sets exposure time in seconds}
 ds_scitc(4),                 {Sets integration time constant for source comp channel}
 d_run(1),                    {Initiates acquisition of data with current mode setting}
 replot_window(),             {Updates the active plot window}
 c1[count1] =dg_scmp(),       {Puts value of source comp channel in c1 array}
 find_peaks(),                {Calls procedure to find peaks in the spectrum}
```

```
 count1 = count1+1,                {Increments the curve count}
end,

{The following procedure assigns values to the variables defined previously}
procedure set_var,
begin
 buflen = 10,
 com_port = 1,    { Set to 1 for COM1 or 2 for COM2 depending on which port is being used}
 numlines = 0,
 center = 0,
 range = 0,
 range1 = 0,
 range2 = 0,
 range3 = 0,
 center1 = 0,
 center2 = 0,
 center3 = 0,
 count1 = 0,
 a1 = 0,
 b1 = 0,
 a2 = 0,
 b2 = 0,
 a3 = 0,
 b3 = 0,
 c1 =0,
 r = 0,
 c = 0,
 d = 0,
 e = 0,
 k = 0,
 l = 0,
 m = 0,
 curve = 0,
 press = 0,
 keyhit = 255,
end,
```

```
{The following procedure receives a W from the NF90 which indicates that it is waiting for the go
command to proceed to next step of command line}
procedure get_w,
begin
 count2 = 0,                          {Initialises the counter variable}
 repeat                               {Repeats until condition is satisfied}
  rsp_byte = 255,                     {Sets the response variable to a default value}
  rsp_byte = g_port(port_address)     {Reads response from com port}
  writeln(),
  write('rsp byte = ',rsp_byte),      {Writes response to screen}
  count2 = count2+1,                  {Increments counter}
  sdelay()
 until (count2>500) or (rsp_byte=87) or((rsp_byte=94) and (count2>10)),
{Repeat read from port until counter reaches 500 or W is received or ^ is received and counter is over 10}
 if (count2>=500) then                {If loop has iterated 500 times inform user}
  begin
   writeln(),
   write('count2= ',count2),
  end,
 if (rsp_byte=94) then                {If ^ received inform user}
 begin
  writeln(),
  write('ready prompt recieved in w loop press enter'),
  readln(),
  check =1                            {Set Program finish flag to 1}
 end,
end,

{The following procedure gets the ^ KEY from the NF90 which indicates that the program of commands
previously loaded has finished executing}
procedure get_term
begin
 check = 0,
 count2 = 0,
 rsp_byte =255,                       {Sets response variable to default value}
 repeat
  rsp_byte  = g_port(port_address)    {Read response from com port}
  writeln(),
  write('term byte = ',rsp_byte)
  sdelay()
 until  (rsp_byte=94),
 if (rsp_byte=94) then
```

```
begin
 writeln(),
 ldelay(),
 write('ready prompt recieved in get term loop press enter'),
 readln(),
 check =1,                          {Set program finish flag to 1}
end,
end,

{The following procedure sends the "G" (go) command as an ASCII character to the NF90}
procedure send_g,
begin
 snd_byte = 71, {G}
 transmit(),
end,

{The following procedure sends a "V" as an ASCII character to the NF90 to verify the controller status}
procedure send_v,
begin
 snd_byte = 86, {V}
 transmit(),
end,

{The following sends a "K" as an ASCII character to the NF90 which kills the operation being executed}
procedure send_k,
begin
 snd_byte = 75, {k}
 transmit(),
end,

{The following procedure sends the command line to the NF90 as a string of ASCII characters
  C S1M1000,S2M1000 B1 L-0,I1M200,U6,L11,I2M200,L-10,R}
procedure send_command,
begin
 snd_byte = 67, {C clears all stored commands from memory}
 transmit(),
 snd_byte = 32, {space}
 transmit(),
 snd_byte = 83, {S SmMx command sets speed of motor m to x steps per second}
 transmit(),
 snd_byte = 49, {1 refers to motor number 1}
 transmit(),
```

```
snd_byte = 77, {M}
transmit(),
snd_byte = 49, {1}
transmit(),
snd_byte = 48, {0}
transmit(),
snd_byte = 48, {0}
transmit(),
snd_byte = 48, {0}
transmit(),
snd_byte = 44, {,}
transmit(),
snd_byte = 83, {S  sets speed of motor 2}
transmit(),
snd_byte = 50, {2}
transmit(),
snd_byte = 77, {M}
transmit(),
snd_byte = 49, {1}
transmit(),
snd_byte = 48, {0}
transmit(),
snd_byte = 48, {0}
transmit(),
snd_byte = 48, {0}
transmit(),
snd_byte = 44  {,}
transmit(),
snd_byte = 66, {B  Bx sets backlash compensation, on if x=1, off if x=0}
transmit(),
snd_byte = 49, {1}
transmit(),
snd_byte = 44, {,}
transmit(),
snd_byte = 76, {L  Sets the loop to marker to this point in the program}
transmit(),
snd_byte = 45, {-}
transmit(),
snd_byte = 48, {0}
transmit(),
snd_byte = 44  {,}
```

```
transmit()
snd_byte = 73, {I ImMx move motor m through x steps in the positive direction}
transmit()
snd_byte = 49, {1}
transmit(),
snd_byte = 77, {M}
transmit(),
snd_byte = 50, {2}
transmit(),
snd_byte = 48, {0}
transmit(),
snd_byte = 48, {0}
transmit(),
snd_byte = 44, {,}
transmit(),
snd_byte = 85, {U U6 causes NF90 to send a W back to the host computer and wait for G to continue}
transmit(),
snd_byte = 54, {6}
transmit(),
snd_byte = 44, {,}
transmit(),
snd_byte = 76, {L Lx, loop x-1 times from loop-to-marker}
transmit(),
snd_byte = 49, {1}
transmit(),
snd_byte = 49, {1}
transmit(),
snd_byte = 44, {,}
transmit(),
snd_byte = 73, {I ImMx move motor m through x steps in the positive direction }
transmit(),
snd_byte = 50, {2}
transmit(),
snd_byte = 77, {M}
transmit(),
snd_byte = 50, {2}
transmit(),
snd_byte = 48, {0}
transmit(),
snd_byte = 48, {0}
transmit(),
snd_byte = 44, {,}
```

```
transmit(),
snd_byte = 76, {L L-x, Loop from the loop to marker x-1 times alternating the direction of motor 1}
transmit(),
snd_byte = 45, {-}
transmit(),
snd_byte = 49, {1}
transmit(),
snd_byte = 48, {0}
transmit(),
snd_byte = 44, {,}
transmit(),
snd_byte = 82, {R Run the program}
transmit(),
end,

{following sends the CLEAR command line as a string of ASCII characters------}
procedure send_clear,
begin
snd_byte = 67, {C Clear program from memory}
transmit(),
snd_byte = 32, {space}
transmit(),
snd_byte = 73, {I ImM0, move motor m (1) to absolute zero position}
transmit(),
snd_byte = 49, {1}
transmit(),
snd_byte = 77, {M}
transmit(),
snd_byte = 48 {0}
transmit(),
snd_byte = 44, {,}
transmit(),
snd_byte = 73, {I Move motor 2 to absolute zero position}
transmit(),
snd_byte = 50, {2}
transmit(),
snd_byte = 77, {M}
transmit(),
snd_byte = 48, {0}
transmit(),
snd_byte = 44, {,}
transmit(),
```

```
 snd_byte =  82,  {R  Run progam}
 transmit(),
end,
{following sends the SETUP command line as a string of ASCII characters------}
procedure send_setup,
begin
 snd_byte =  70,  {F  Enable on-line mode with echo off}
 transmit(),
 snd_byte =  78,  {N  Null or zero the absolute position registers of motors 1,2 and 3}
 transmit(),
end,

{following sends the QUIT command as a string of ASCII characters------}
procedure send_quit,
begin
 snd_byte =  81,  {Q  Quit on-line mode}
 transmit(),
end,
{The following procedure sends the commands to the NF90 to clear all previous commands and return the
table to its original position}
procedure finish,
begin
  send_clear(),
  writeln(),
  write('Sending clear line'),
  get_term(),
  send_quit(),
  writeln(),
  write('Sending quit line')
end,
{The following procedure allows the user to cancel the scan at any point by hitting the ESC key  If this
key is pressed then the commands, which the NF90 is currently executing, are killed and the table is
returned to its original position}
procedure breakout,
begin
    buflen =20,
     if keypressed then              {If a key has been pressed do the following}
     begin
      keyhit  = readch()             {Record the key which was pressed}
      write('keyhit=',keyhit),       {Write the value to the screen}
      delay()
      if keyhit = 129 then           {If it was the ESC key do the following}
```

```
      begin
       writeln(),                    {Write a message to the screen to show that program is terminating}
       write('program termination requested by user    '),
       delay(),
       send_k(),                     {Terminate all previous commands to NF90}
       get_term(),                   {Receive confirmation that commands are terminated}
       finish(),                     {Call procedure to finish map and return NF90 to origin}
       check =1,                     {Set flag to show that map is finished or terminated}
       writeln(),
       write('program terminated by user!'),
      end,
     end,
end,
{End of procedures}
{Main program starts here}
begin
 set_var(),                          {Initialise the variables before use}
 if (com_port = 1) then              {This section defines which port to send data }
  port_address = 1016                { to and defines the port address in memory   }
 else if (com_port = 2) then
  port_address =  760
 else error(),                       {If a com port other than 1 or 2 is selected there is an error}
 if err= 0 then                      {If there are no errors do the following}
 begin
  check = 0,                         {Set program finish flag to initial value 0}
  writeln(),
  buflen =18,
  write('setting up x-y table'),
  ldelay(),
  send_setup(),                      {Send command to set up the x-y table for use}
  ldelay(),
  rsp_byte  = g_port(port_address),  {Receive response from NF90}
  writeln(),
  write('rsp byte = ',rsp_byte),     {Write NF90 response to screen}
  ldelay(),
  writeln(),
  write('sending command line')
  delay(),
  send_command(),                    {Send command to define the mapping procedure of the NF90}
  breakout(),                        {Check for user request to exit program}
  set_lines(),                       {Set the parameters for the data analysis of spectra}
 while check <> 1  do                {While program finish flag is not set to 1 do the following}
```

```
 begin
 get_w(),                    {Receive W from NF90}
 breakout(),                 {Check for user request to exit program}
 if keyhit <> 129 then       {If ESC key has not been pressed do the following}
  begin
  if check <> 1 then         {If program finish flag is not set to 1 do the following}
   begin
   scan(),                   {Call procedure to perform scan }
  end,
  send_g(),                  {Send go command to NF90}
  send_v(),                  {Verify status of NF90}
 end,
end,
if keyhit <> 129 then        {If the ESC key has not been pressed do the following}
 begin
 save_to_file(),             {Save the data collected to file}
 writeln(),
 write('count = ',count1),   {Inform user of the number of data points in the scan}
 finish(),                   {Call procedure to finish map and return x-y table to origin}
 delay(),
 writeln(),
 buflen =47,
 write('end of program')     {Inform the user that the program has finished}
 end,
end,
end

{End of program}
```

Appendix B

Source Compensation System

The source compensation system described here was designed and built to work in conjunction with the OMA-Vision CCD system This CCD had a source compensation input on its A/D board via a BNC connector This connection received an analog signal proportional to the excitation level during a measurement The input to this connection was a voltage in the range 0 to +10 V for integrated mode or 0 to +6 V for non-integrated operation The input impedance was 10 KΩ and the signal was delivered by a 50 Ω coaxial cable from the external detector Depending on the choice of modes, the signal was directly digitised (Sample) or integrated for a defined time period ranging from 10 μs to 1 s (Integrate)

A detector and ancillary electronics were designed and built to monitor laser power and deliver a signal in the appropriate range to the CCD board The detector was placed in the excitation beam path to monitor the excitation level during operation In this way any fluctuations of laser power that occurred while measurements were being made could be normalised out of the resulting spectra Consequently the intensities of corresponding peaks in different spectra could be correlated

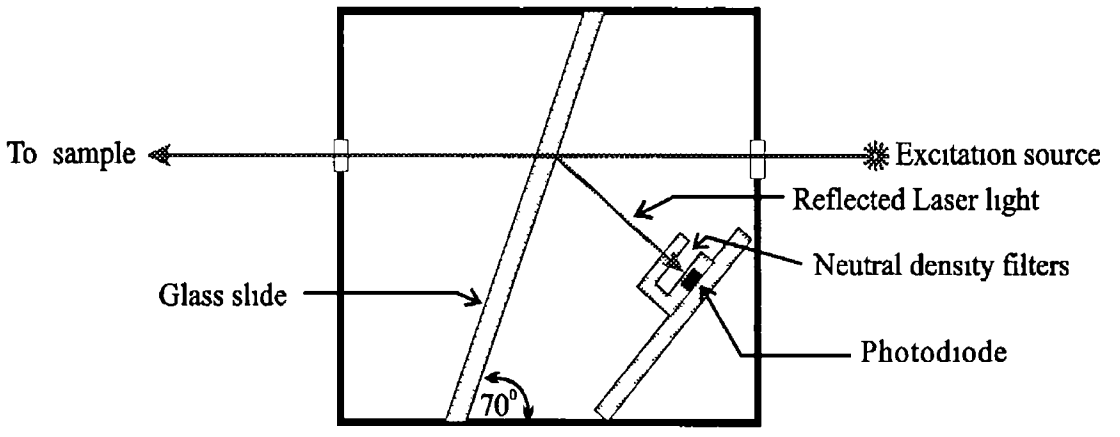

Fig B1 Schematic diagram of the detector arrangement for excitation source intensity level monitoring

The detector was based on a Texas Instruments TSL250 light-to-voltage optical sensor This device was a monolithic silicon IC containing photodiode, operational

amplifier and feedback components The required electronic components to power this device and convert the resulting signal to that appropriate for the CCD were also built The laser beam was sampled using a glass slide which back-reflected a small proportion of the incident radiation The reflected beam passed through an adjustable set of neutral density filters before illuminating the photodiode A schematic diagram of the detector head is shown in fig B1 The combination of neutral density filters and adjustable electronic amplification scales allowed a wide range (~10 mW to 1 W) of input light intensities to be sampled

The source compensation system was tested for linearity of response and for its ability to normalise a fluctuating signal caused by variations in laser power The system was found to have a very linear voltage to input power response and was also able to compensate for even large fluctuations to within 0 01% This slight variation occurred at the transitional points when the fluctuations were rapid which would not typically occur in a stable laser system This shows that the compensation system should be sufficient to deal with any source fluctuation occurring under normal operating conditions